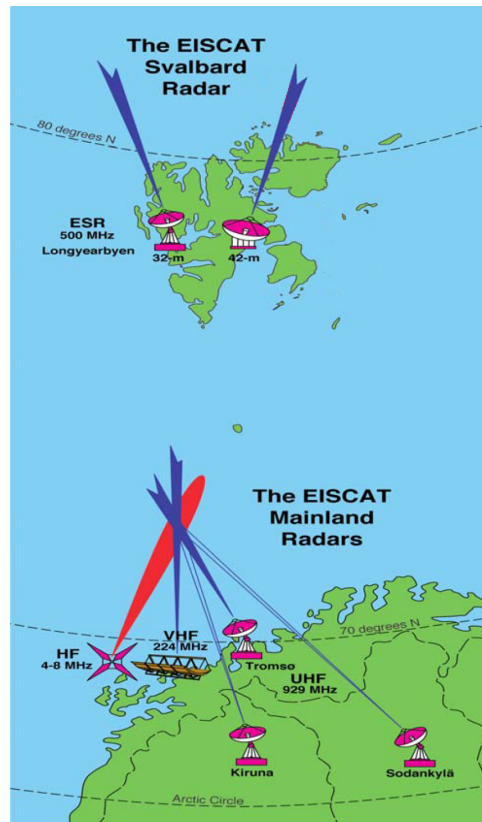


EISCAT

EUROPEAN INCOHERENT SCATTER
SCIENTIFIC ASSOCIATION

ANNUAL REPORT 2009



EISCAT Radar Systems

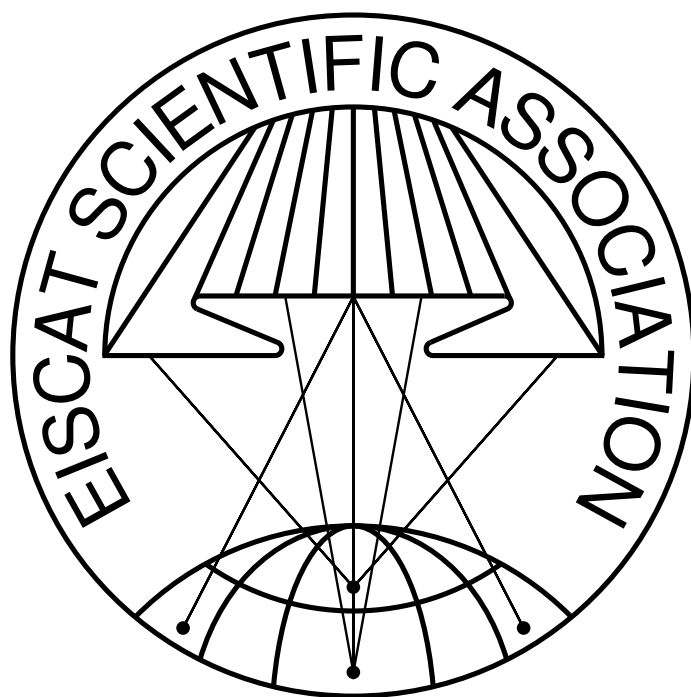
Location	Tromsø		Kiruna	Sodankylä	Longyearbyen	
Geographic coordinates	69°35'N 19°14'E		67°52'N 20°26'E	67°22'N 26°38'E	78°09'N 16°01'E	
Geomagnetic inclination	77°30'N		76°48'N	76°43'N	82°06'N	
Invariant latitude	66°12'N		64°27'N	63°34'N	75°18'N	
Band	VHF	UHF	UHF	UHF	UHF	
Frequency (MHz)	224	931	931	931	500	
Maximum bandwidth (MHz)	3	8	8	8	10	
Transmitter	1 klystron	2 klystrons	-	-	16 klystrons	
Channels	8	8	8	8	6	
Peak Power (MW)	1.6	2.0	-	-	1.0	
Average power (MW)	0.20	0.25	-	-	0.25	
Pulse duration (ms)	0.001–2.0	0.001–2.0	-	-	0.0005–2.0	
Phase coding	binary	binary	binary	binary	binary	
Minimum interpulse (ms)	1.0	1.0	-	-	0.1	
Receiver	analog		analog	analog	analog	
System temperature (K)	250–300		90–110	50	65–80	
Digital processing	14 bit ADC, 32 bit complex, autocorrelation functions, parallel channels				12 bit ADC, lag profiles 32 bit complex	
Antenna	parabolic cylinder 120 m × 40 m steerable	parabolic dish 32 m steerable	parabolic dish 32 m steerable	parabolic dish 32 m steerable	Antenna 1 parabolic dish 32 m steerable	Antenna 2 parabolic dish 42 m fixed
Feed system	line feed 128 crossed dipoles	Cassegrain	Cassegrain	Cassegrain	Cassegrain	Cassegrain
Gain (dBi)	46	48.1	48.1	48.1	42.5	44.8
Polarisation	circular	circular	any	any	circular	circular

EISCAT Heating Facility in Tromsø

Frequency range: 4.0–8.0 MHz, Maximum transmitter power: 12 × 0.1 MW, Antennas: Array 1 (5.5–8.0 MHz) 30 dBi, Array 2 (4.0–5.5 MHz) 24 dBi, Array 3 (5.5–8.0 MHz) 24dBi.

Additionally, a Dynasonde is operated at the heating facility.

Cover picture: Artist's view of a future EISCAT_3D active site.



EISCAT Scientific Association
2009

EISCAT, the European Incoherent Scatter Scientific Association, is established to conduct research on the lower, middle and upper atmosphere and ionosphere using the incoherent scatter radar technique. This technique is the most powerful ground-based tool for these research applications. EISCAT is also being used as a coherent scatter radar for studying instabilities in the ionosphere, as well as for investigating the structure and dynamics of the middle atmosphere and as a diagnostic instrument in ionospheric modification experiments with the heating facility.

There are eleven incoherent scatter radars in the world, and EISCAT operates three of the highest-standard facilities. The experimental sites of EISCAT are located in the Scandinavian sector, north of the Arctic Circle. They consist of two independent radar systems on the mainland, together with a further radar constructed on the island of Spitzbergen in the Svalbard archipelago — the EISCAT Svalbard Radar — Scandinavia (see schematic and operating parameters on the inside of the front cover).

The EISCAT UHF radar operates in the 931 MHz band with a peak transmitter power of 2.0 MW and 32 m, fully steerable parabolic dish antennas. The transmitter and one receiver are in Tromsø (Norway). Receiving sites are also located near Kiruna (Sweden) and Sodankylä (Finland), allowing continuous tri-static measurements to be made.

The monostatic VHF radar in Tromsø operates in the 224 MHz band with a peak transmitter power of 1.6 MW and a 120 m × 40 m parabolic cylinder antenna, which is subdivided into four sectors. It can be steered mechanically in the meridional plane from vertical to 60° north of the zenith; limited east-west steering is also possible using alternative phasing cables.

The EISCAT Svalbard radar (ESR), located near Longyearbyen, operates in the 500 MHz band with a peak transmitter power of 1.0 MW, a fully steerable parabolic dish antenna of 32 m diameter, and a fixed field aligned antenna of 42 m diameter. The high latitude location of this facility is particularly aimed at studies of the cusp and polar cap region.

The basic data measured with the incoherent scatter radar technique are profiles of electron density, electron and ion temperature, and ion velocity. Subsequent processing allows a wealth of further parameters, describing the ionosphere and neutral atmosphere, to be derived. A selection of well-designed radar pulse schemes are available to adapt the data-taking routines to many particular phenomena, occurring at altitudes between about 50 km and more than 2000 km. Depending on geophysical conditions, a best time resolution of less than one second and an altitude resolution of a few hundred meters can be achieved.

Operations of 3–4000 hours each year are distributed equally between Common Programmes (CP) and Special Programmes (SP). At present, six well-defined Common Programmes are run regularly, for between one and three days, typically about once per month, to provide a data base for long term synoptic studies. A large number of Special Programmes, defined individually by Associate scientists, are run to support national and international studies of both specific and global geophysical phenomena.

Further details of the EISCAT system and operation can be found in various EISCAT reports, including illustrated brochures, which can be obtained from EISCAT Headquarters in Kiruna, Sweden.

The investments and operational costs of EISCAT are shared between:

*China Research Institute of Radiowave Propagation, Peoples Republic of China
Deutsche Forschungsgemeinschaft, Germany
National Institute of Polar Research, Japan
Norges forskningsråd, Norway
Science and Technology Facilities Council, United Kingdom
Solar-Terrestrial Environment Laboratory, Nagoya University, Japan
Suomen Akatemia, Finland
Vetenskapsrådet, Sweden*

Contents

The Council Chairperson's section	7
Director's pages	8
The EISCAT_3D Design Study	12
Scientific highlights 2009	14
Ionospheric studies	14
On the source of the polar wind in the polar topside ionosphere: First results from the EISCAT Svalbard radar	14
Characteristics of polar patches in the nightside ionosphere	14
The influence of ozone concentration on the lower ionosphere	15
Particle precipitation during NEIAL events: simultaneous ground based nighttime observations at Svalbard	15
Omega band electrodynamics	16
Characteristics of ion upflow and downflow observed with the European Incoherent Scatter Svalbard radar	17
Statistics of Joule heating, electric fields and conductances	17
Studies in the D-region	18
D-region electron density and effective recombination coefficients during twilight and solar proton events	18
Dynamics of the precipitation regions causing auroral radio absorption	19
Auroral studies	19
Small-scale auroras: Flickering and black auroras	19
Electric field enhancement in an auroral arc	20
Relations between proton auroras, intense electric field and ionospheric electron density depletion	20
Studies of the cusp	21
Ion heating in high-speed flow channel within the duskside cell of the polar-cap ion convection under large IMF- B_y condition	21
Cusp observations during a series of fast reversals of the interplanetary magnetic field	21
Moving meso-scale plasma precipitation in the cusp	22
Studies of polar mesosphere summer echoes	23
Radio Physics of PMSE	23
Frequency dependence of polar mesosphere summer echoes	23
The layered dust plasma structure of PMSE	23
Studies involving artificial ionospheric heating	24
HF heating campaigns by AARI	24
Artificial modification of polar mesospheric winter echoes with the EISCAT Heater and the role of charged dust particles	27
Polar ionospheric heating	28
F-region electron heating by X-mode radiowaves	28
Ionospheric modification and plasma physics	29

Studies of the thermosphere	30
Temperature enhancements and vertical winds in the lower thermosphere associated with auroral heating during the Dynamics and Energetics of the Lower Thermosphere in Aurora (DELTA) campaign	30
Meso-scale thermospheric response	31
Acceleration mechanism of high-speed neutral wind observed in the polar lower thermosphere	31
DELTA-2 campaign: Study of the energetics and the wind dynamics in the polar lower thermosphere	32
Studies of dust and meteorites	32
Measurements of meteor smoke particles during the ECOMA-2006 campaign	32
High statistics radar meteor studies at EISCAT	33
Signatures of mesospheric particles in ionospheric data	34
Solar wind studies	34
Interaction a between medium-scale transient in the solar wind and a stream interaction region	34
Theoretical studies of incoherent scattering spectra	35
20-moment approximation for ion velocity distribution and its application in calculations of incoherent scatter spectra	35
Incoherent scatter spectra of collisional plasma	35
List of publications 2009	37
EISCAT Operations 2009	40
Beynon medals	44
EISCAT organisational diagram 2009	45
Committee Membership and Senior Staff	46
Appendix: EISCAT Scientific Association Annual Report, 2009	49
The EISCAT Associates, December 2009	63
Contact Information	64

The Council Chairperson's section

The transition from the traditional EISCAT activities to preparatory work for a new radar system — including major upgradings both in the mainland radars and in Svalbard — was the most important topic in the work of the EISCAT Council during 2009. The performance of the VHF radar continued to be below optimal as only one of the klystrons was in use. On the other hand, the plans for renovation work were in fair wind. The EISCAT_3D concept was accepted to the ESFRI Road Map at the end of 2008 and the EU-funded Design Study for the 3D concept ended successfully in spring 2009. In addition, China made a very fascinating proposal to extend the ESR system with a third antenna dish.

The composition of the EISCAT Association and its management structures were discussed several times in the Council meetings. In particular, the role of the EISCAT Management Committee (EMC) was reconsidered. The wish from the new Director, Dr. Esa Turunen, was that this Committee would provide him a link towards the Council not only during the Council meetings. The discussions in the Council and EMC finally led to a solution where EMC was renamed Council Advisory Group (CAG) and its tasks in the Statutes were reformulated. CAG's role is to advise the Council on matters related to administrative issues, development of facilities and the Association, finances, legal issues, planned operations and other items relevant for the Council. Both the Director and the Council chairperson participate in the CAG work. The Council supporting roles of SOC (Scientific Oversight Committee) and CAG are different: SOC can give its recommendations entirely from the basis of scientific argumentation while CAG's task is to evaluate SOC's recommendations from the viewpoint of the available resources in the Association. For this reason it was recommended that both SOC and CAG would arrange their gatherings before the Council meetings and in such a timeframe that CAG can take into account the SOC output in its recommendations to the Council.

The criteria for full versus associate membership are under continuous discussion because dur-

ing recent years some old member countries have decided to leave EISCAT and new partners are stepping in. The re-organization of UK science funding structures in 2009 had an impact also to the EISCAT management and economy situation which further complicated the picture. In an additional Council meeting arranged as a telecom at the end of 2009, the opportunities for the UK to make some changes in its representatives and commitments for the Association were discussed extensively. The negotiations for Ukraine's membership in EISCAT continued in 2009 and as a transition period solution EISCAT made a one-year collaboration agreement with this country. Russia continued collaboration with the Association by buying significant amount of observing time and the links towards the Russian science community were strengthened by inviting a Russian representative to SOC. In the Council discussions it was noted that the long-term commitments are essential for the core operations of the Association and for this reason they can be considered as the cornerstone criterion for a full membership status. On the other hand, joining EISCAT should be attractive and easy also for countries whose science funding is organized in shorter cycles than the five year cycle used in the EISCAT membership rules. In this controversial situation it is still important to guarantee fair and equal treatment for all members in the Association.

The practice where a staff representative participates in the Council meetings was tested during the year 2008. This practice ended in 2009 because the staff had expressed the opinion that the presence of their representative is needed only when the Council needs the staff opinion to guide its solutions. The Council decided to accept this change, but on the other hand it encouraged the staff to continue the biennial selection of a staff representative. The wish is to continue the dialogue between staff and the Council and the message from the Council Chairperson is that both sides can serve as the initiator in this discussion.

*Dr. Kirsti Kauristie
Chairperson of the EISCAT Council*

Director's pages

As in January 2009 I was handed over the responsibility of the daily management and operation of the facilities of the EISCAT Scientific Association, as the new Director, I felt strong confidence: first, on the continuing capacity of the Association being able to serve its users for their scientific needs in providing measurement opportunities at the modern ISR operational level, and second, in inspiring and motivating its user community to develop the ISR method towards a brand new future. The future had been outlined during the achievements in the soon to be finished EISCAT_3D Design Study. This confidence was not only based on my earlier experience as a user of the EISCAT radars; having been the PI of many Finnish radar campaigns through the years, I had met devoted, committed and skilful staff at the sites. Similar feelings were passed to me while meeting the enthusiasm and guidance given by the various active EISCAT Committee members, starting at the last year's Council meeting in Kunming, China, throughout the year in the Science Oversight and EISCAT Management Committee meetings. Specially the previous director Tony van Eyken, Prof. Asgeir Brekke and Dr. Kirsti Kauristie, the previous and new Council chairs respectively, stood by my side as immediate support, using a lot of their time when guiding me into how the activities of the association are to be seen in international context.

But the most significant strengthening of my confidence on the strengths of EISCAT appeared in the beginning of the year, when the EISCAT staff gathered for its Annual Review meeting in Pallas-tunturi in Finland on 11–13 February. Staff reports of the technical status of the various parts of our distributed facilities impressed me in dedication, detail and honest evaluation. I was confirmed that EISCAT has its most important resource in the existing staff, all doing their best at highest possible level of expertise and with experience gained through many, many years of operation and maintenance tasks. As EISCAT had gone through several successful upgrades during the history, the core competence to take similar renewal actions

for the future, is at place already. It would be my task to ensure that this competence would not be lost with possibly restricted financial resources foreseen in the near future and that there would be ways to find new resources, which could be directed towards the next renewal. The total number of EISCAT staff however had been cut during the recent years to a minimum, which would not last too many unexpected losses. Even now some part of preventive maintenance had to be abandoned, simply due to less manpower available. However, all technical problems appearing at the sites during the year were solved with minimum delays, and the overall maintenance task appeared to be manageable at all the sites. As EISCAT is a distributed facility located in the territory of three different countries, Sweden, Finland, Norway and Svalbard, the large distances set up some specific demands in internal communication. We decided to establish some new meetings, such as twice a year a site leader meeting, where leading staff from Headquarters and from all the sites would meet physically for one day discussions. Naturally the internal site meetings were encouraged. These were regularly held at the sites but were missing at the Headquarters and were introduced there. Also the EISCAT scientists decided to have virtual meetings, testing a few times internet-based conference solutions. However, the conclusion of these tests was that with our various connections and hardware set-ups, still at this phase a standard teleconference by ordinary phones is the most reliable virtual meeting method.

The association is facing some changes, which should be seen as opportunities to renew significantly within few years in future. Russia successfully conducted EISCAT experiments during their affiliate agreement, where they essentially buy experiment time similar to what France is doing. The Russian contribution is at an essential level financially and an agreement is written for three years. With Ukraine we had a minor level agreement, which made the first purely Ukrainian EISCAT experiments possible. This was a one year arrangement at this stage, but continuation is expected.

The long-standing EISCAT Associate Science and Technology Facilities Council (STFC) in the UK informed EISCAT that by end of 2009, the UK associateship would be transferred to the National Environment Research Council (NERC). At this stage of the transfer, which includes some negotiations within Council, an agreement with NERC is being signed to start as the UK associate from 2010. We thank STFC for the extensive work during the years, as generally known, the UK has led many developments in EISCAT in the past. At the same time we welcome NERC to continue the work and possibly bring in new fields of their interests to the EISCAT activities.

European Union has been funding access to EISCAT facilities in the TransNational Access program, which ended in 2009. The TNA program did not reach its planned target, there were fewer users than anticipated. As there is currently no foreseen similar funding appearing in Europe, one could ask if there could be an EISCAT funded TNA-type program available in the future? An option would be combine this somehow with the current third party proposals. In any case TNA has succeeded in bringing new countries to the user list of EISCAT. One should continue in creating opportunities for these research groups who have learnt to know EISCAT, in order to be able to create an enlarging and collaborating EISCAT user community simply because the ISR method, data analysis and sophisticated combined use of ISR data with other measurements, are concepts which will take some time for any individual to master.

Operations in 2009 were reduced as compared to the previous year. This occurred naturally, since in 2008 one still had the International Polar Year operations running. The annual measurement hours were 3688 in total. The Tromsø VHF radar is running with one klystron only. The repaired one is kept as a reserve currently, since the EISCAT Site Leaders meeting in May 2009 estimated a 7 months break in operations to be the result if the second klystron would be taken into use. The Tromsø site has suffered from limited engineering manpower, but this is now helped by hiring a new engineer Jan Børre Henriksen. The Tromsø scientist Dr. Lisa Baddeley left EISCAT in July 2009, in order to work as the SPEAR scientist at UNIS. At the heating upgrade in Tromsø, there are still issues to be solved, but the work is ongoing. Heating suffers from small amount of technical support staff, which would be needed to help the responsible Senior Scientist. The Tromsø engineers are devoting part of their time in order to support Heat-



ing maintenance. It should be also noted here that in addition to the Dynasonde in Tromsø, EISCAT also has a Dynasonde in operation on Svalbard, and all the Dynasonde data are available on the internet. At the remote sites Kiruna and Sodankylä, we are still having three persons at each site, but there is a reduction foreseen soon, as in 2010 we will have one staff retirement at both sites. Refilling these positions is not anticipated since we expect diminishing operations. The receiver frequency protections will end at both sites in 2010.

EISCAT continued some exceptional observations in 2009. Beyond standard ISR operations one could mention the space debris detections after the Iridium-Cosmos satellite collision in spring 2009. The Iridium cloud orbital plane passes as well as the Cosmos cloud passes are clearly identifiable in data, which could be used to improve the current statistical model. The Finnish EISCAT user group introduced also the use of non-uniform interpulse periods to receive echoes from all altitudes. In these experiments efficient space debris and ISR measurements can be combined. Typical EISCAT measurements leave over 50% of the ranges blank because the transmission and ground clutter always block echoes from the same ranges for each transmission. Just now we are not foreseeing any more space debris measurements, unless European Space Agency is requesting related operations.

EISCAT users are in the process of setting up some extraordinary instrumentation at the radar sites: The Japanese lidar installation at the Tromsø site includes three container houses. When in operation the lidar laboratory would be a major optical instrument to be used with EISCAT radars for

the next ten years. The interferometer at ESR site is currently under refurbishment and a new data acquisition is being installed. First operational data is expected next year.

Year 2009 marked the successful finishing of the 4-year long EU-funded Design Study of the EISCAT_3D radar concept. In December 2008, the European Strategy Forum on Research Infrastructures, ESFRI, had selected EISCAT_3D on its Roadmap of strategically important infrastructures. As proposed facilities on this Roadmap should be attractive for the global science community for the next 20–30 years, but located in Europe, EISCAT had gained a good science political starting point with the EISCAT_3D concept. The proposal was submitted by Swedish Research Council as the initiator, and interestingly, EISCAT_3D was placed in the Environmental group of RI projects. A similar ESFRI status was given at the same time to a Norwegian proposal, The Svalbard Integrated Arctic Earth Observation System, SIOS, where research activities from the bottom of the sea up to the upper atmosphere and geospace, based on the existence of measurements and measurement sites in the Svalbard area, were proposed to be strengthened and coordinated internationally as a concerted but interdisciplinary effort. The EISCAT Svalbard radar would be an essential part of the upper atmospheric research programme of SIOS. SIOS was in a very similar development stage as the EISCAT_3D proposal, the next step would be to apply funds for a preparatory phase action with selected partner institutions. Such a preparatory phase should solve all issues before construction of the new research infrastructure: legal, governance, strategic, financial and, if necessary, technical work should be directed towards making it possible to go to construction phase directly after the preparatory phase. As EU opened a financing call to support preparatory phases of the ESFRI Roadmap projects, EISCAT decided to hire Dr. Ian McCrea from Rutherford Appleton Laboratory in part time, in order to coordinate writing a targeted funding application. A full time position of a project assistant was also established and Dr. Anders Tjulin started to work at EISCAT Headquarters in Kiruna in September 2009. The finalising of a 6 M€ funding application was conducted during an intensive workshop with a small team of international contributors, and the application was sent to EU in December 2009.

A dedicated first international EISCAT_3D User Meeting was organised in Uppsala on 27–29 May 2009, hosted by the Swedish Institute of Space

Physics, Uppsala, in the premises of the Ångström Laboratory. The purpose of the meeting was twofold: first, to offer opportunity to EISCAT users to show their plans and needs for measurements in their science fields, second, to publish the results of the EISCAT_3D Design Study to the wide user community. The results of the Design Study were formally handed over to EISCAT in the meeting by the partner consortium representative, the technical coordinator of the study: Dr. Gudmund Wannberg from Swedish Institute of Space Physics in Kiruna. Final reports of the Study were submitted to EU afterwards and these reports are available to anyone via the EISCAT and EISCAT_3D web pages. Dr. Wannbergs earlier work for the EISCAT radars in general as well as the recent work for the EISCAT_3D Design Study were given a recognition in the 73rd EISCAT Council meeting in Lillehammer on 27–28 November 2009, when he was awarded with the 7th Beynon medal.

In spring 2009 we restarted discussion with the frequency authorities of all EISCAT Host Countries, Norway, Sweden and Finland. Our main discussion was of course in order to ensure future operations of EISCAT_3D, but also current facilities were discussed, specially because timing the possible ending of current frequency licenses should match opportunity to use the new EISCAT_3D frequency. Norway is currently offering the 229.9–236.6 MHz to EISCAT, as a response to the application sent out during the EISCAT_3D Design Study. We have replied this to be fine for us, but so far there is no confirmation from the authority. Finland shows support to protect the band in Northern Finland for EISCAT, provided the location(s) of measurement site(s) are in areas where this would be possible. Sweden has future allocation to DAB (digital audio broadcast) development, but there are several authorities involved in making decisions. Swedish Research Council offers to coordinate discussions with these authorities. The frequency allocation of EISCAT_3D should be solved as soon as possible, since this is one of the prerequisites before the technical realisation of the new generation radar can be brought forward.

A showcase of all the EISCAT science was the 14th EISCAT Workshop on 3–7 August 2009, in Tromsø, Norway. The number of participants was this time slightly less than during previous workshops, in total 85, but included a very international mix of participants from all over the world. Among more traditional ses-

sions such as, space weather and solar wind-magnetosphere-ionosphere-atmosphere coupling, high-latitude ionospheric response, mesosphere and thermosphere, meteors and space debris, ionospheric modification, and new techniques, also sessions on the future with EISCAT_3D and use of the enhancing global ISR network were organised. During the latter, the workshop participants were introduced a new conceptual need in future geosciences: a more system-oriented approach and holistic view of the whole geospace environment and Earth itself as a composite system, where one finally needs a more global approach both to measurements and modelling efforts. At the EISCAT workshop in Tromsø, the user community of EISCAT had a discussion on how to develop further the access to EISCAT data archive. Parallel to the standard MADRIGAL database use, EISCAT had started in 2008 to introduce a new opportunity, based on dedicated extensive software development on a hardware platform consisting of six computers transferred to EISCAT Kiruna site from Rutherford Appleton Laboratory. A software consultant had worked on this system for 5.5 months to March 2009, in order to create a more elegant data access system, with extensive metadata searches to access raw data, re-analysis of data collected by these metadata searches etc. As EISCAT itself did not allocate more resources to the combined software/hardware platform development, the next step was agreed to be taken by the user community, by applying and developing the system to fulfil needs of their selected science cases. It remains to be seen if such an alternative resource via user engagement is enough to bring the system to be a standard user level tool.

The next EISCAT International Workshop in 2011 will be held in China. China has made an ambitious project proposal to EISCAT, as a possible in-kind contribution to EISCAT in the form of a third antenna on Svalbard. Originally the EISCAT Svalbard radar was proposed optimally to have three antennas. Finally one was built and only later another one was added as the Japanese in-kind contribution. Initial technical description of the proposed third antenna is now given by the Chinese associate CRIRP. This is similar to the 50 m antenna of the Chang'e Moon project in Beijing, and indeed the idea proposed is to use the antenna for multiple purposes, including ISR and Space Debris measurements and communication with the Chinese Moon projects, using both a separate transmitter at S band and the existing ESR transmitter at 500 MHz. The Science Oversight

Committee of EISCAT, SOC, finalised a document on the science case of the third antenna; SOC recommends this addition to ESR. Several delegations from China visited Tromsø and Longyearbyen in order to discuss and map the case of the third antenna. Also initial discussions were made with a consultant who could serve in casting the project into an action, including possible feasibility study and communication with local authorities on construction and operation permissions. The next phase would be to make a decision on taking such initial steps towards the realisation of the third antenna.

Another possible development on Svalbard appeared during the Svalbard Science Forum, where international research institutes who are active in Svalbard area, gathered to discuss on coordinative actions. In fact EISCAT proposed to start collaborative work towards a similar effort as was done during the last International Polar Year in 2007–2008, a coordinated continuous measurement period, at least one year long, during the next solar maximum. This would be possibly around 2013. Such an operation with ESR is a major undertaking, and demands extra funding. The IPY operations with EISCAT were done using extreme effort by EISCAT staff, also helped by others. As learned from that experience, dedicated extra engineering staff would be needed to be hired at the required level. Without funding coming outside of the EISCAT standard budget, the continuous solar maximum operation will not be possible.

Although some minor reduction in resources available to EISCAT in the nearest future may happen, I still think the current view towards future is much enlightened. We have the EISCAT_3D concept, which is having a political backing in Europe, and is certainly also of global science interest. With coordinated science-led development, both within and beyond the EISCAT community, and applied both in Svalbard, where the SIOS ESFRI project and the Chinese third antenna proposal may develop further the traditional strengths in order to address new science, as well as on mainland, where the Heater upgrade should bring in new developments in small-scale physics, and novel applications, such as planetary radar and space debris measurement capability, enhanced data access and finally the EISCAT_3D ESFRI project, all should develop new techniques to add new science. With this view in mind, I would like to thank the EISCAT staff for their excellent work in 2009.

*Dr. Esa Turunen
Director, EISCAT Scientific Association*

The EISCAT_3D Design Study

In 2009 the four-year EISCAT_3D Design Study was completed. This project was supported by the Sixth Framework Programme of the European Union and was running from 1 May 2005 to 30 April 2009.

The aims of the Design Study were essentially twofold:

- To study the feasibility of constructing a third-generation incoherent scatter research radar, using cutting-edge technology throughout and providing an order-of-magnitude improvement in temporal and spatial resolution so that the existing, aging, EISCAT VHF and UHF systems, could be replaced.
- To produce a detailed costed design for such a system.

The Design Study did not include a task to develop the science case; this was carried out as a parallel activity by EISCAT's Science Advisory Committee (SAC), later renamed as the Science Oversight Committee (SOC) from 1 January 2007. Members of the Design Study maintained close links with the science case development, and many of the ideas from SAC fed into the preparation of the EISCAT_3D Performance Specification Document (PSD).

Following extensive consultation with the scientific user community in 2004 and 2005, it was determined that only a multi-static phased array system could reach or approach the performance demanded by present users and expected from future users.

Accordingly, the target system specified in the EISCAT_3D Performance Specification Document (PSD) comprises a central active (transmit-receive) site (the "core") and four receive-only sites, located on two approximately 250 km long baselines oriented North-South and East-West, respectively.

To achieve the desired performance, the proposed system design incorporates a number of innovative ground-breaking concepts such as

- Direct-sampling receivers.

- Digital time-delay beam-forming.
- Multiple simultaneous beams from each receiving array.
- Adaptive polarisation matching and Faraday rotation compensation.
- Digital arbitrary-waveform transmitter exciter system.
- Full interferometry and imaging capabilities.
- Amplitude-domain data recording at full sampling rate.

During the four-year Design Study, all mission-critical technical concepts were modelled, investigated by simulations and in critical cases also by full-scale tests, and found to be realisable. Array sizes, transmitter power levels and receiver noise performance that would be required to reach the desired time and space resolutions have also been established. Based on this work, the target system was proposed to have the following technical characteristics:

The EISCAT_3D core should comprise a 120 m diameter filled circular aperture array with about 16,000 elements (see Fig. 1), laid out on an equilateral triangular grid, and in addition a number (six to nine) of smaller outlier receive-only arrays. It would then provide

- Half-power beamwidth of about 0.75° which is comparable to that of the present EISCAT UHF.
- Power-aperture product exceeding 100 GWm^2 which is an order of magnitude greater than that of the present EISCAT VHF.
- Grating-lobe free pattern out to 40° zenith angle.
- Graceful degradation in case of single-point equipment failure.



Figure 1: Artist's view of the EISCAT_3D core site as proposed in the Design Study.

Each core array element should be made up from a radiator, a dual 2×300 W linear RF power amplifier, a high performance direct-digitising receiver and support electronics. The recommended radiator is a crossed Yagi antenna with a minimum directivity of about 7 dBi.

Two filled 8000 element receive-only arrays should be installed on each baseline at distances of about 110 and 250 km from the core, respectively. Their radiating elements will be three- or four-element X Yagis, essentially identical to those used in the core. The Yagis would be directed towards the core field-of-view and elevated to 45° . Outlier arrays for interferometry should also be installed at the receive-only sites.

Advanced digital beam-forming systems would allow the generation of a large number of simultaneous beams from each array, thus eliminating the time/space ambiguity plaguing all present incoherent scatter systems and realise the possibilities for volumetric imaging of vector quantities for the first time.

It was verified that a system meeting the performance requirements put forth in the EISCAT_3D Performance Specification Document could be built today, using existing technology, if cost were not an issue. Advances in semiconductor technology, signal processing and data storage between now and the time of placing a contract are expected to reduce component and subsystem costs to the point where a full-size core would cost

about 60 M€ and each receive-only site 20 M€. It is recommended that the member institutions of the EISCAT Scientific Association commit to funding and constructing such a radar system according to the results and guidelines given in the technical reports (EISCAT_3D Deliverables) within the next five to seven years.

As designed, the system would be highly modular and would lend itself excellently to gradual expansion if funding should only be forthcoming in installments. In this case, it is recommended that in a first phase a 5000 element, 70 m diameter core array and at least two 1500 element receiver sites should be constructed to replace the multi-static capabilities of the present UHF radar, which are going to be lost in 2010. This configuration would already exceed the performance of the current VHF system, providing a 1.3° half-power beamwidth, a power-aperture product of about 10 GWm^2 , and full beam steerability at the transmitter site. There are also stages beyond the outlined system involving multiple core elements arrays that could then be expanded as additional funding became available or as part of a more comprehensive initial build.

The Design Study team notes with pleasure that, as a result of their efforts and the hard work of the EISCAT executives, EISCAT_3D was added to the European Strategy for Research Infrastructure (ES-FRI) roadmap, at its last revision announced in December 2008.

Scientific highlights 2009

Ionospheric studies

On the source of the polar wind in the polar topside ionosphere: First results from the EISCAT Svalbard radar

In this study, we present quantitative radar observations of both hydrogen ion (H^+) and oxygen ion (O^+) upflow in the topside polar ionosphere (Fig. 2) using measurements that were recently carried out with the EISCAT Svalbard Radar and the Reimei satellite. H^+ upflow was clearly observed equatorward of the cusp above 500 km altitude. Within the cusp the H^+ density was very low, and the upflow was dominated by O^+ ions, but on closed field lines the H^+ became the larger contributor to the upward flux above about 550 km. The total flux seemed to be conserved, and so below 550 km altitude O^+ (with a small upward velocity of ~ 50 m/s) appeared to determine the upward flux which was then maintained by H^+ in the topside ionosphere. We also found that the H^+ density in the topside polar ionosphere was several times higher than current predictions of ionospheric models like IRI2001.

Y. Ogawa, et al., "On the source of the polar wind in the polar topside ionosphere: First results from the EISCAT Svalbard radar", *Geophysical Research Letters* 36, L24103, doi:10.1029/2009GL041501, 2009.

Characteristics of polar patches in the nightside ionosphere

The characteristics of polar patches in the European nightside ionosphere have been investigated. These patches are the remnants of ionospheric plasma originating on the dayside and drawn anti-sunward across the polar region into the nightside auroral region.

A multi-instrument study using the ESR, the Aberystwyth radio tomography experiment, and the SuperDARN radars observed the modulation of patch separation during a magnetic substorm.

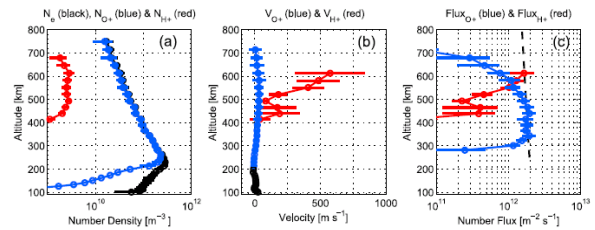


Figure 2: Height profiles equatorward of the cusp of H^+ , O^+ , and total electron density (panel a), H^+ and O^+ upward velocities (panel b), and H^+ and O^+ upward number fluxes (panel c). In panel c the thick dashed lines indicate constant flux extended in height from the observed peaks for a dipole magnetic field.

During substorm expansion the patches were separated by some 5° latitude but this was reduced to some 2° when activity had subsided. The different patch separations resulted from the expansion and contraction of the high-latitude plasma convection pattern on the nightside in response to the substorm activity. The patches of larger separation occurred in the anti-sunward cross-polar flow as it entered the nightside sector from the polar region. Those of smaller separation were also in anti-sunward flow, but close to the equatorward edge of the convection pattern, in the slower, diverging flow of the Harang discontinuity. A patch repetition time of some 10 to 30 min was estimated depending on the phase of the substorm.

A second multi-instrument study investigated the influence of the season on the patch-to-background density ratio in the nightside ionosphere around solar maximum (1999–2001). Patch-to-background ratios of up to 9.4 ± 2.9 were observed by the ESR between midwinter and equinox with values of up to 1.9 ± 0.2 in summer. The patch-to-background ratios in summer were less than two, so the enhancements could not formally be called patches, nevertheless they were identified as significant density enhancements within the antisunward cross-polar flow. Modelling of the difference between winter and summer patch-to-background ratios primarily at-

tributed the variation to the chemical composition of the atmosphere, which in summer both reduced the electron densities of the plasma drawn into the polar cap on the dayside and enhanced plasma loss by recombination. A secondary factor was the maintenance of the background polar ionosphere by photo-ionisation in summer.

A. G. Wood, S. E. Pryse, and J. Moen, "Modulation of nightside polar patches by substorm activity", *Annales Geophysicae* 27(10), 3923–3932, 2009.

A. G. Wood, and S. E. Pryse, "Seasonal influence on polar cap patches in the high-latitude nightside ionosphere", *Journal of Geophysical Research*, in press, 2010.

The influence of ozone concentration on the lower ionosphere

A numerical model of D-region ion chemistry is used to study the influence of the ozone concentration in the mesosphere on ion-composition and electron density during solar proton events (SPE). We find a strong sensitivity in the lower part of the D-region, where negative ions play a major role in the ionisation balance. We have chosen the strong SPE on 29–30 October 2003 when very intense proton fluxes with a hard energetic spectrum were observed. Deep penetration into the atmosphere by the proton fluxes and strong ionisation allows us to use measurements of electron density, made by the EISCAT 224 MHz radar, starting from as low as 55 km. We compare the electron density profiles with model results to determine which ozone concentration profiles are the most appropriate for mesospheric altitudes under SPE conditions (Fig. 3). We show that, during daytime, an ozone profile corresponding to depletion by a factor of 2 compared to minimum model concentrations for quiet conditions (Rodrigo et al., 1986), is needed to give model electron density profiles consistent with observations. Simple incorporation of minor neutral constituent profiles (NO, O and O₃) appropriate for SPE conditions into ion-chemistry models will allow more accurate modeling of electron and ion densities during such events, without the need to apply a complete chemical model calculating all neutral species.

A. Osepian, S. Kirkwood, and P. Dalin (2009), "The influence of ozone concentration on the lower ionosphere — modelling and measurements during the 29-30 October 2003 solar proton event", *Annales Geophysicae* 27(2), 577–589, 2009.

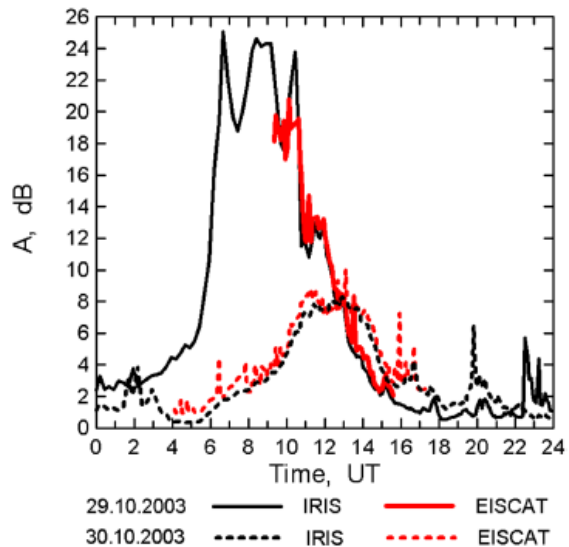


Figure 3: Comparison of time series of the measured values of cosmic noise absorption from the IRIS riometer at Kilpisjärvi (black curves) with absorption calculated on the basis of experimental (EISCAT) N_e -profiles (red curves). The solid lines are on 29 October 2003, the dashed lines are on 30 October 2003. Absorption is given for a frequency of 30 MHz.

Particle precipitation during NEIAL events: simultaneous ground based nighttime observations at Svalbard

In this investigation it was discovered for the first time that Natural Enhanced Ion Acoustic Lines (NEIALs) may occur during night time at high latitudes over Svalbard. The geophysical settings indicate that the NEIAL events in this case study are associated with the substorm expansion phase on the nightside. We have also found that the green line may exceed the red line intensity during NEIAL events, causing enhancement in the up-shifted shoulder in the incoherent scatter spectra. This shows that both soft and hard precipitation is essential for the generation of NEIALs; the harder precipitation being important for the enhancement in the up-shifted ion-acoustic line. We also find that the enhancement of the down-shifted shoulder is not strictly related to the previously found threshold of about 10 kR for the 630.0 nm line intensities. There seems to be a possible link between the NEIAL events and the 844.6 nm line emission intensity which probably makes this line a more suitable indicator of NEIAL activity than the 630.0 nm emission line. Both the 630.0 nm

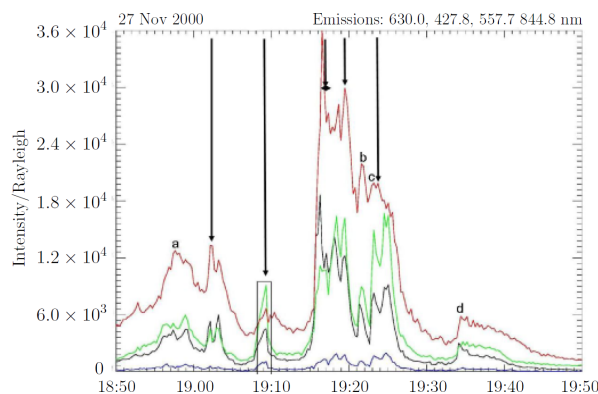


Figure 4: The optical emissions arriving from the field aligned direction coinciding with the radar beam. NEIAL events are marked with black arrows (and a black diamond), while the notation a, b, c and d marks emission peaks during which no NEIAL events were observed.

and 844.6 nm are emitted by atomic oxygen (OI), excited by low energy precipitation, but the latter results from a prompt emission, and shows a better correlation with NEIALs on the short time scales involved which makes this line a good candidate as an optical signature of NEIALs. Figure 4 shows the optical emissions arriving from the field aligned direction coinciding with the radar beam. NEIAL events are marked with black arrows (and a black diamond), while the notation a, b, c and d marks emission peaks during which no NEIAL events were observed. The enclosed frame illustrates a case when the green line intensity exceeds the red line. Figure 5 shows the NEIAL event with an enhanced right shoulder at the time when the green emission line exceeded the red line.

J. Lunde, U. P. Løvhaug, and B. Gustavsson, "Particle precipitation during NEIAL events: simultaneous ground based nighttime observations at Svalbard", *Annales Geophysicae* 27(5), 2001–2010, 2009.

Omega band electrodynamics

The study by Vanhamäki et al. (2009) presents a case study of omega band electrodynamics. This study evaluates the performance of the new regional variant of the traditional KRM-method developed by Vanhamäki and Amm (1997). The regional approach uses equivalent current data and conductance values as input and yields estimates of ionospheric electric field and currents as outputs. The contribution from EISCAT comes via conductance estimates: From auroral intensities and riometer data the Hall and Pedersen

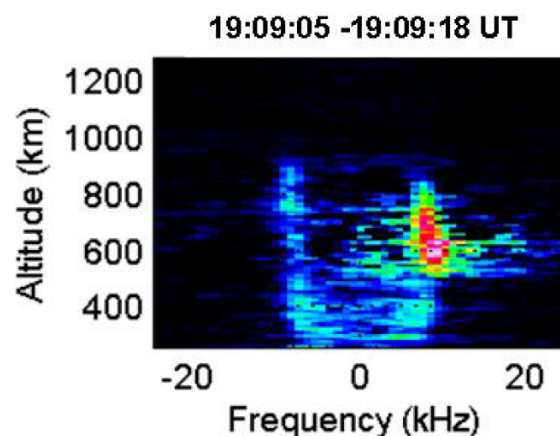


Figure 5: The NEIAL event with an enhanced right shoulder at the time when the green emission line exceeded the red line (the enclosed frame in Fig. 4).

conductances are derived with a semi-empirical model whose development EISCAT observations have supported (Senior et al., 2008). Vanhamäki et al. (2009) show that the electric field maps deduced with the regional KRM method are in general consistent with CUTLASS electric field measurements. The spatial distribution of most intense Joule heating regions in the omega band structure is also investigated and the heating is found to be higher in the dark region than in the auroral tongue (Fig. 6). However, the two auroral tongues analysed in the study have differences in this respect: the heating rates associated with the first auroral tongue are larger than those of the second tongue and of the dark region between the tongues. On the other hand, the first tongue occurred in connection with pseudo-breakup auroras, so its higher Joule heating rates are not surprising. The lesson to learn from this study is that the spatial distribution of Joule heating in omega-bands cannot be deduced on the basis of optical data alone.

A. Senior, M. J. Kosch, and F. Honary, "Comparison of methods to determine auroral ionospheric conductances using ground-based optical and riometer data", *Annales Geophysicae* 26(12), 3831–3840, 2008.

H. Vanhamäki, and O. Amm, "A new method to estimate ionospheric electric fields and currents using data from a local ground magnetometer network", *Annales Geophysicae* 25(5), 1141–1156, 2007.

H. Vanhamäki, et al., "Electrodynamics of an omega-band as deduced from optical and magnetometer data", *Annales Geophysicae* 27(9), 3367–3385, 2009.

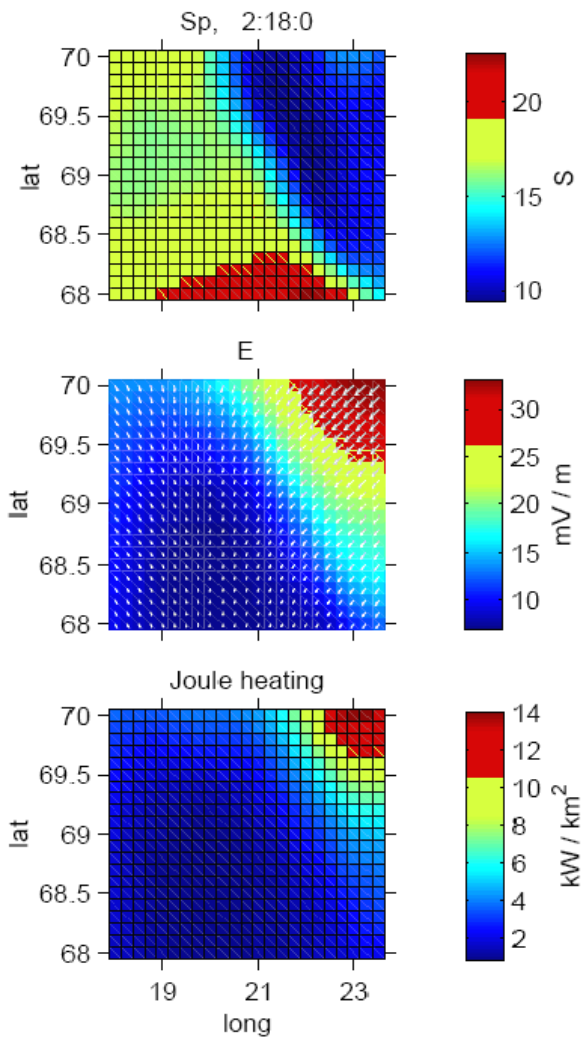


Figure 6: The Pedersen conductance, electric field (vector field and intensity), and Joule heating rate in the vicinity of an omega band structure. The auroral tongue is located in the region of enhanced Pedersen conductances and only a part of the large omega structure is visible.

Characteristics of ion upflow and downflow observed with the European Incoherent Scatter Svalbard radar

In this study, we investigated how geomagnetic activity, the solar wind (SW), and the interplanetary magnetic field (IMF) influence the occurrence of the F-region/topside ionospheric ion upflow and downflow. Occurrence of dayside ion upflow observed with ESR at 75.2° magnetic latitude is highly correlated with the SW density (Fig. 7), as well as with the strength of the IMF B_y component. We suggest that this correlation exists be-

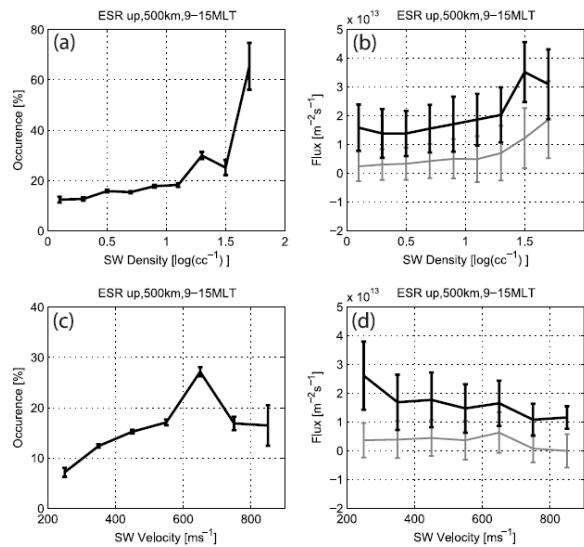


Figure 7: Dayside ion upflow occurrence and ion flux plotted over solar wind (SW) parameters: (a, b) SW density and (c, d) SW velocity. In panels b and d the black lines indicate average fluxes in upflow events, while gray lines indicate average fluxes of all data (upflow, downflow, and no-flow events).

cause the region where ion upflow occurs is enlarged owing to SW density and IMF B_y magnitude, but it does not move significantly in geomagnetic latitude. The occurrence frequency of dayside ion upflow displays peaks versus the geomagnetic activity index (K_p), SW velocity, and negative IMF B_z component; that is, ion upflow is less frequently seen at the highest values of these parameters. Dayside ion downflow in the F-region/topside ionosphere occurs only when the K_p index and/or SW velocity are high or when IMF B_z is largely negative. The results suggest that the region of ion upflow not only becomes larger but also moves equatorward with increasing K_p , SW velocity, and negative IMF B_z . The ESR can so be poleward of the upflow region and observe ions convecting poleward and returning ballistically downward.

Y. Ogawa, et al., "Characteristics of ion upflow and downflow observed with the European Incoherent Scatter Svalbard radar", Journal of Geophysical Research 114, A05305, doi:10.1029/2008JA013817, 2009.

Statistics of Joule heating, electric fields and conductances

Properties of the Joule heating rate, electric fields and conductances in the high latitude ionosphere

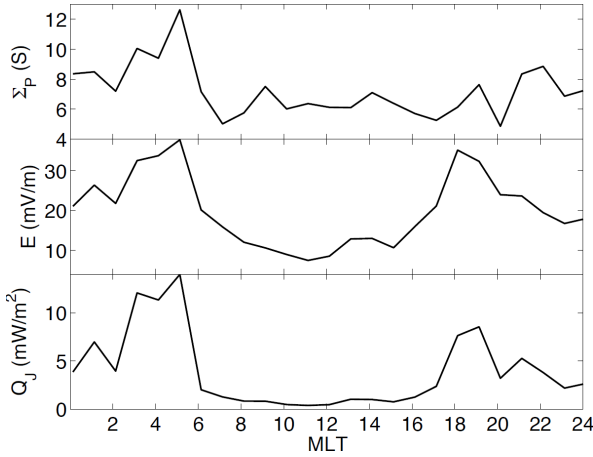


Figure 8: Median curves of Pedersen conductance (top panel), total electric field (middle panel) and Joule heating rate (bottom panel) for $K_p \geq 3$.

are studied by Aikio and Selkälä (2009). The results are based on a one-month measurement made by the EISCAT incoherent scatter radar in Tromsø (66.6 cgmlat) from 6 March to 6 April, 2006. The data are thus from the same season (close to vernal equinox) and from similar sunspot conditions (about 1.5 years before the sunspot minimum) providing an excellent set of data to study the magnetic local time (MLT) and the K_p magnetic activity index dependence of ionospheric parameters with high spatial and temporal resolution.

The results indicate that the response of morning sector conductances and conductance ratios to increased magnetic activity is stronger than that of the evening sector. The co-location of Pedersen conductance maximum and electric field maximum in the morning sector produces the largest Joule heating rates 00–05 MLT for $K \geq 3$ (Fig. 8). In the evening sector, a smaller maximum occurs at 18 MLT, mainly due to an intense electric field. Minimum Joule heating rates in the nightside are statistically observed at 23 MLT, which is the location of the electric Harang discontinuity.

Fits for the Joule heating rate as a function of electric field magnitude, separately for four MLT sectors and two activity levels ($K_p < 3$ and $K \geq 3$) are also performed. In addition to the squared electric field, the fit includes a linear term to study the possible anticorrelation or correlation between electric field and conductance. In the midday sector, positive correlation is found, as well as in the morning sector, for the high activity case. In the midnight and evening sectors, anticorrelation between electric field and conductance is obtained,

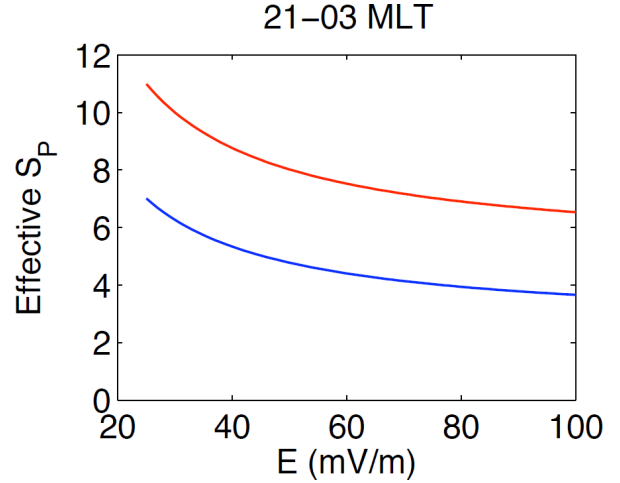


Figure 9: Effective conductance as a function of electric field in the midnight sector for $K_p < 3$ (blue) and $K_p \geq 3$ (red).

i.e. intense electric fields are associated with low conductances (Fig. 9). This is expected to occur in the return current regions adjacent to auroral arcs as a result of ionosphere-magnetosphere coupling. In addition, a part of the anticorrelation may come from polarisation effects inside high-conductance regions, e.g. auroral arcs. These observations emphasise the importance of small-scale electro-dynamics, which is not included in most of the global models of Joule heating rate.

A. T. Aikio, and A. Selkälä, “Statistical properties of Joule heating rate, electric field and conductances at high latitudes”, *Annales Geophysicae* 27(7), 2661–2673, 2009.

Studies in the D-region

D-region electron density and effective recombination coefficients during twilight and solar proton events

Accurate measurements of electron density in the lower D-region (below 70 km altitude) are rarely made. This applies both with regard to measurements by ground-based facilities and by sounding rockets, and during both quiet conditions and conditions of energetic electron precipitation. Deep penetration into the atmosphere of high-energy solar proton fluxes (during solar proton events, SPE) produces extra ionisation in the whole D-region, including the lower altitudes, which gives favourable conditions for accurate measurements using ground-based facilities. In this study we

show that electron densities measured with two ground-based facilities at almost the same latitude but slightly different longitudes, provide a valuable tool for validation of model computations. The two techniques used are incoherent scatter of radio waves (by the EISCAT 224 MHz radar in Tromsø, Norway, 69.6°N, 19.3°E), and partial reflection of radio-waves (by the 2.8 MHz radar near Murmansk, Russia, 69.0°N, 35.7°E). Both radars give accurate electron density values during SPE, from heights 57–60 km and upward with the EISCAT radar (Fig. 10) and between 55–70 km with the partial reflection technique. Near noon, there is little difference in the solar zenith angle between the two locations and both methods give approximately the same values of electron density at the overlapping heights. During twilight, when the difference in solar zenith angles increases, electron density values diverge. When both radars are in night conditions (solar zenith angle >99°) electron densities at the overlapping altitudes again become equal. We use the joint measurements to validate model computations of the ionospheric parameters f^+ , λ , α_{eff} and their variations during solar proton events. These parameters are important characteristics of the lower ionosphere structure which cannot be determined by other methods.

A. Osepian, et al., “D-region electron density and effective recombination coefficients during twilight — experimental data and modelling during solar proton events”, *Annales Geophysicae* 27(10), 3713–3724, 2009.

Dynamics of the precipitation regions causing auroral radio absorption

The analysis of D-region observations by the VHF radar in March 2008 investigated the dynamics of the precipitation regions causing auroral radio absorption. The motions were monitored by the imaging riometer at Kilpisjärvi. From the EISCAT data the height of the absorbing layer was determined, and hence the energy of the precipitating electrons causing the absorption. The gradient-curvature drift of electrons of these energies would be much greater than the speeds observed. Magnetospheric circulation, as inferred from SuperDARN, is a more promising mechanism, though as yet unproven.

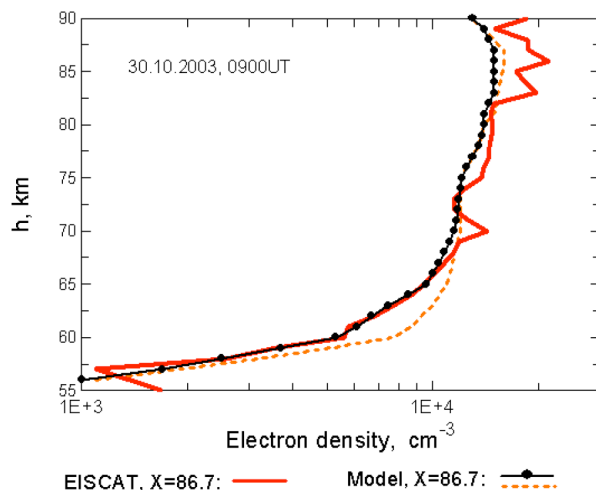


Figure 10: Electron density profiles measured by EISCAT radar (red curve) and calculated for the SPE on 30 October 2003 at 09:00 UT for zenith angle 86.7° (black curve) using different models of O, O₃ and NO profiles (black and red dashed curves).

Auroral studies

Small-scale auroras: Flickering and black auroras

A study of two flickering auroral events using the ASK (Auroral Structure and Kinetics) multi-spectral imaging system in combination with the UHF radar has led to improved understanding of the mechanism responsible for flickering aurora (Fig. 11). Several ‘chirps’ were identified within the events, in which the frequency of flickering ascended or descended over a short period of time (~1–2 s). By observing different optical emission lines it was found that the energy of precipitation is inversely proportional to the flickering frequency over the duration of each chirp. This is predicted by the theory that flickering aurora is a result of the Landau damping interaction between electrons and electromagnetic ion cyclotron (EMIC) waves, and that the wave speed is the primary factor determining the electron energy gain.

The ASK imager has also been used in conjunction with the UHF radar to study the dynamics and energy characteristics of so-called ‘black aurora’. The flux reduction of high energy particles versus low energy particles in the black regions compared to the diffuse background have been investigated for different forms of black aurora. Two separate mechanisms have been suggested to cause black aurora. The larger reduction of high energy precipitation within the fine scale

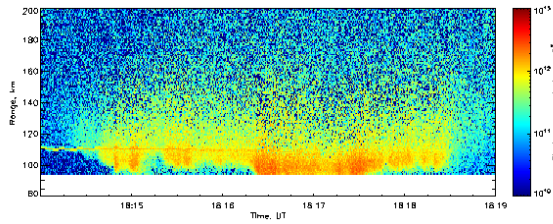


Figure 11: UHF radar high resolution data. The flickering aurora occurred between 18:16:30 and 18:17:30 UT and corresponds to higher energy particle precipitation causing ionisation to lower altitudes.

black structures favours a magnetospheric mechanism that blocks high energy electrons from being scattered into the loss cone.

D. K. Whiter, et al., "Using multi-spectral optical observations to discriminate between possible acceleration mechanisms for flickering aurora", *Journal of Geophysical Research*, submitted, 2010.

J. Archer, et al., "Dynamics and characteristics of black aurora as observed by high resolution ground-based imagers and radar", *International Journal of Remote Sensing*, submitted, 2010.

Electric field enhancement in an auroral arc

The character of a change in the ionospheric electric field when several auroral arcs crossed the region of radar measurements has been analysed (Fig. 12). In one case the plasma conductivity and electric field normal component in an arc increased as compared to their undisturbed values. In another case the field and conductivity changed traditionally (in antiphase). Arcs with an increased field were previously classified as correlating arcs, but their existence was subsequently open to question during optical observations. The usage of the ALIS system of digital cameras made it possible to decrease the errors introduced by optical equipment. The measurements in the vicinity of correlating arcs were performed when these arcs were generated, and a traditional arc was a completed formation. In an originating arc, the field value can depend not only on the ionospheric plasma conductivity but also on the processes in the magnetospheric-ionospheric system resulting in the field enhancement.

V. V. Safargaleev, et al., "Electric field enhancement in an auroral arc according to the simultaneous radar (EIS-

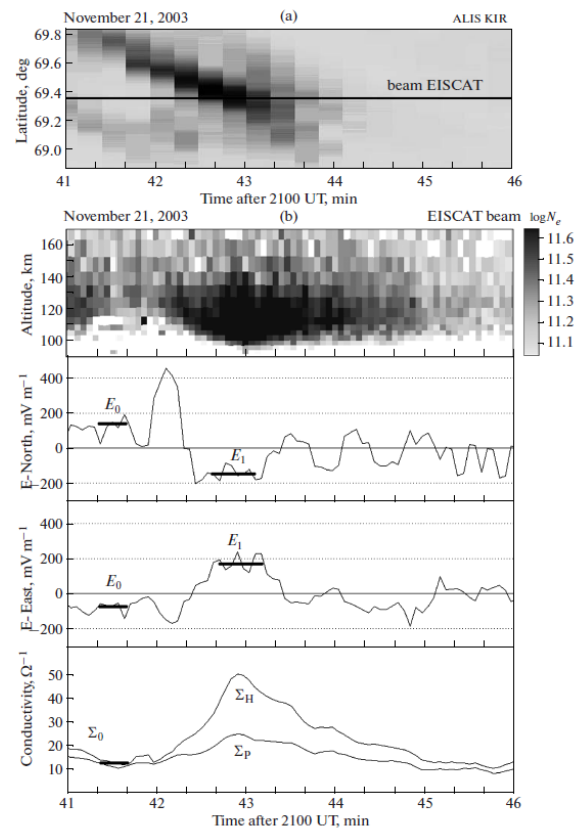


Figure 12: Optical and radar measurements in the vicinity of the correlating arc.

CAT) and optical (ALIS) observations", *Geomagnetism and Aeronomy* 49(3), 353–367, 2009.

Relations between proton auroras, intense electric field and ionospheric electron density depletion

A case study with simultaneous European Incoherent Scatter and optical auroral observations was conducted in order to determine characteristics of the magnetosphere-ionosphere coupling from the viewpoint of the electrodynamics in the ionosphere. Particular focus was on the relationships between ionospheric electron density depletion, perpendicular electric fields, and proton auroras. Intense electron density depletion was observed in the E and F regions poleward and in the vicinity of a thin equatorward moving arc (Fig. 13). This depletion was associated with an intense, equatorward perpendicular electric field close to ~ 80 mV/m and most likely with a downward field-aligned current (FAC), but it did not accompany detectable proton aurora. Hence the down-

ward FA electric field in the lower magnetosphere associated with this depletion was weak or absent. The motion of the FAC system with the depletion and the arc presumably enabled the downward FAC to obtain enough current carriers as ionospheric electrons were lost by the evacuation process. The evacuation process associated with the downward FAC was, however, efficient enough to establish the depletion. On the other hand, a widely distributed proton aurora observed immediately after the depletion was associated with an intense, equatorward perpendicular electric field close to 90 mV/m, enhanced electron density, and most likely a downward FAC. No electron precipitation was associated with this proton aurora. Thus the electron density enhancement, providing the downward current carriers, had to be caused by the ionization of precipitating protons presumably accelerated by downward field-aligned electric fields in the lower magnetosphere.

R. Fujii, et al., "Relations between proton auroras, intense electric field and ionospheric electron density depletion", *Journal of Geophysical Research* 114, A09304, doi:10.1029/2009JA014319, 2009.

Studies of the cusp

Ion heating in high-speed flow channel within the duskside cell of the polar-cap ion convection under large IMF- B_y condition

F region strong sunward ion flow embedded in the duskside cell of expanding polar cap ion convection and coincidental increase in the ion temperature were observed using the European Incoherent Scatter (EISCAT) radars at Tromsø, Sodankylä and Longyearbyen together with the CUTLASS HF radars. The convection map obtained by the SuperDARN HF radars showed that the high-speed flow channel elongated in 14–17 MLT was moving equatorward. The increase of the measured ion temperature at the common scattering volume of the EISCAT radars was in good agreement with the ion frictional heating estimated under the assumption of the null neutral wind velocity for about 20 min, and then it became much lower than the estimate of the ion frictional heating. While the flow channel moved equatorward, the ion temperature increase became less evident at higher part of latitudes within the flow channel, which means that ion frictional heating was

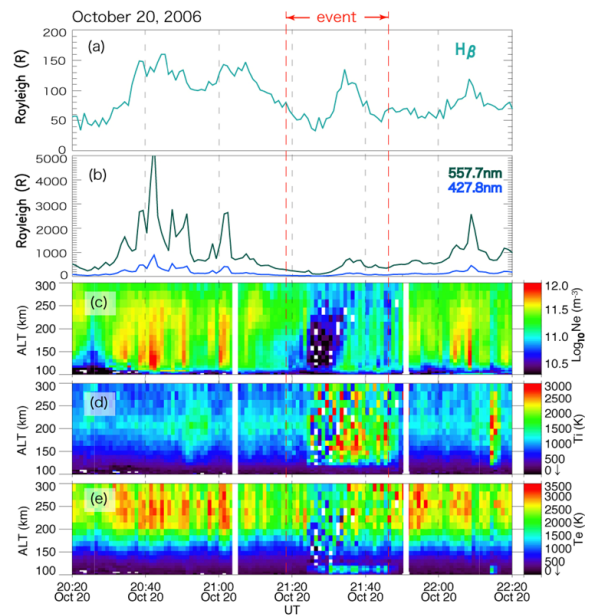


Figure 13: A summary plot of the time variations of several parameters between 2020 and 2220 UT on 20 October 2006. From the top to bottom, (a) $H\beta$ emissions from the proton aurora imager, (b) electron auroral emissions at 427.8 and 557.7 nm from the photometer, (c) the height profile of the electron density along the magnetic field line, (d) the ion and (e) electron temperatures from the EISCAT radar. The interest for the present study is an event around 2130 UT.

depressed where the neutral gases had already responded to the high-speed ions. The increase in the ion temperature at particular geomagnetic latitude continued until the neutral wind was accelerated to the equivalent level of the surrounded ion flow (Fig. 14).

S. Maeda, et al., "Ion heating in high-speed flow channel within the duskside cell of the polar-cap ion convection under large IMF- B_y condition", *Journal of Geophysical Research* 114, A11307, doi:10.1029/2009JA014300, 2009.

Cusp observations during a series of fast reversals of the interplanetary magnetic field

A comparative study of the cusp was performed, focusing on an interval in which the IMF B_z component underwent four reversals, remaining for around 30 minutes in each orientation. The Cluster spacecraft were on an outbound trajectory through the northern hemisphere magnetosphere, whilst the VHF and ESR were operating. The series of IMF reversals resulted in a sequence of pole-

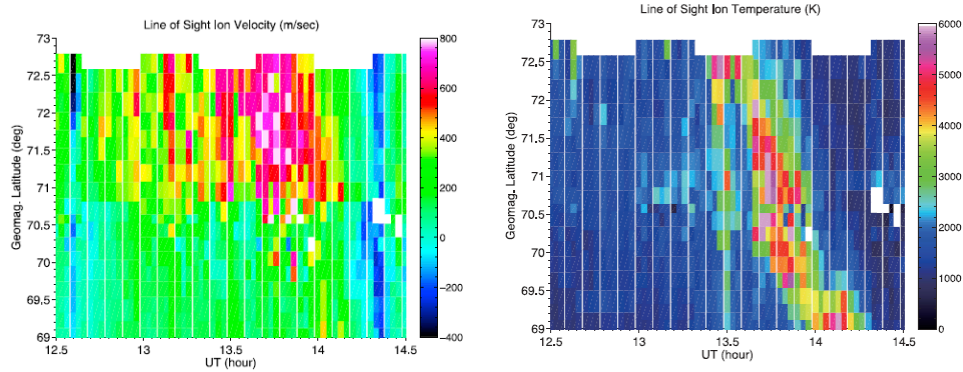


Figure 14: Plots of the line-of-sight ion velocity (left) and temperature (right) as a function of geomagnetic latitude and UT. The TRO data in the latitudes lower than the common scattering volume (70.5° – 71.0°) is combined with the ESR data in the latitudes higher than the volume. The positive value of the ion velocity represents velocity away from the Tromsø radar and towards the ESR. The enhancements of the line-of-sight ion velocity and temperature appeared in the highest latitudes at 13:30 UT and propagated to the lower latitudes. The increase of the line-of-sight ion temperature at particular geomagnetic latitude started almost simultaneously with the enhancements of the line-of-sight ion velocity. It continued for about 20 min and then ceased before the end of the ion velocity enhancement.

ward and equatorward motions of the cusp. Consequently Cluster crossed the high-altitude cusp twice before finally exiting the dayside magnetopause, both times under conditions of northward IMF B_z . The first magnetospheric cusp encounter, by all four Cluster spacecraft, showed reverse ion dispersion typical of lobe reconnection. Subsequently, Cluster spacecraft 1 and 3 crossed the cusp for a second time. During this second cusp crossing, these two spacecraft were likely to have been on newly closed field lines, which were first reconnected (opened) at low latitudes and later reconnected again (re-closed) poleward of the northern cusp.

H. T. Cai, et al., “Cusp observations during a series of fast IMF B_z reversals”, *Annales Geophysicae* 27(7), 2721–2737, 2009.

Moving meso-scale plasma precipitation in the cusp

On 28 March 2001, when the interplanetary magnetic field was strongly duskward, the DMSP F12 spacecraft observed an ion precipitation burst in a latitudinally narrow region near 1200 MLT. A few minutes earlier, the Low Energy Neutral Atom (LENA) imager on the IMAGE spacecraft, whose field of view (FOV) looks into the high-altitude cusp, detected an enhancement of energetic neutral atom signals, which are produced by the ion injection. The LENA data suggest that the ion injection moved out of its FOV after approximately

4 min. At this time, the ground-based magnetometers of the IMAGE chain in Svalbard, located westward of LENA’s FOV, began to indicate perturbations. These perturbations immediately reached a peak and then ceased; the perturbations lasted 2–3 min. During this interval, there was an enhanced westward flow over Svalbard, as observed by the SuperDARN radars. The EISCAT Svalbard radar detected an enhancement of electron density and temperature that was concurrent with this flow enhancement, suggesting that a plasma precipitation burst accompanied with the flow. These observations, which cover a longitudinally extending region of the cusp, strongly suggest the existence of moving mesoscale plasma precipitation (MMPP). The MMPP travels westward with a longitudinally elongated form. Its leading and trailing edges should be created by the temporal effect of the cusp. The other edges, which lie along the streamline, would originate in a spatially limited region along the open-closed line. The boundary of the MMPP form is delineated by both the temporal and spatial structures of the cusp.

S. Taguchi, et al., “Moving meso-scale plasma precipitation in the cusp”, *Journal of Geophysical Research* 114, A06211, doi:10.1029/2009JA014128, 2009.

Studies of polar mesosphere summer echoes

Radio Physics of PMSE

Using the small scale structure of electron density caused by charged dust particles, the following relation between the volume reflectivity and frequency occurring Polar Mesosphere Summer Echoes (PMSE) was obtained

$$\eta = R^2 \Theta_{1/2}^{-2} L^{-1} = \left(\frac{\Delta N_e r_e c^2}{2\pi f^2} \right)^2 e^{-\frac{\pi^2 \ln 2}{2}} \Theta_{1/2}^{-2} L^{-1},$$

where ΔN_e denotes the absolute step of electron density, r_e the classical electron radius, $\Theta_{1/2}$ one-way half-power half width, c the speed of light and L the radar pulse width. Meanwhile, the statistical result

$$\eta = 3.8 \times 10^{-5} \times f^{-4.37}$$

was obtained.

Also, by analysing the data obtained from ECT-02, one can find that the dusty plasma in polar summer mesopause is weakly ionised and weakly coupling. The stronger disturbance of the electron density corresponds to the stronger radar echoes.

H. Li, et al., "One analysis on the rocket detection of polar mesosphere summer echoes", Chinese Journal of Space Science 29(4), 397–401, 2009.

H. Li, et al., "Study on the relation between the reflectivity and frequency in dusty plasma of polar summer mesopause", Plasma Science and Technology 11(3), 279–282, 2009.

Frequency dependence of polar mesosphere summer echoes

The frequency dependence of polar mesosphere summer echoes (PMSE) has been observed using simultaneous and common volume measurements. Detailed observations using the EISCAT Svalbard radar (ESR, 500 MHz) and the SOUSY Svalbard radar (SSR, 53.5 MHz) located near Longyearbyen on Svalbard (78°N, 16°E) were presented by Li et al. (2009a,b). The campaign was conducted during the polar summer in 2006 and the backscattered signal of the radars were converted to absolute volume reflectivities (radar cross-section per unit volume) which is a system-independent parameter. Figure 15 shows the measured volume reflectivities obtained from ESR/SSR measurements during periods of the

occurrence of PMSE. From the experimentally derived volume reflectivity ratios together with modelled volume reflectivity profiles for turbulent scatter can be revealed that PMSE is indeed created by turbulent scatter in the presence of large Schmidt number (Li et al., 2009a). Further investigations have been conducted and result in particle size distributions inside the PMSE layers which has been recently published by Li et al. (2010).

Q. Li, et al., "Frequency dependence of PMSE: Results from simultaneous and common volume measurements with EISCAT radars", in Proceedings containing extended abstracts of twelfth workshop on technical and scientific aspects of MST radar, edited by W. Hocking, London, ON Canada, May 17–23, 2009a.

Q. Li, et al., "Microphysical parameters of mesospheric ice clouds derived from calibrated PMSE observations at 53.5 MHz and 500 MHz", in The 9th international workshop on Layered Phenomena in the Mesopause Region, Stockholm, Sweden, July 12–15, 2009b.

Q. Li, et al., "Microphysical parameters of mesospheric ice clouds derived from calibrated observations of polar mesosphere summer echoes at Bragg wavelengths of 2.8 m and 30 cm", J. Geophys. Res. 115, D00I13, doi:10.1029/2009JD012271, 2010.

The layered dust plasma structure of PMSE

The rocket experimental data indicated that the layered dusty plasma structure has a sharp boundary in the summer polar mesopause. In order to combine with the experimental results, traditional hydrodynamic equations and charging equation is adopted to build physical models of the dusty plasma to study the physics process about the sharp boundary in the stratified structure. The theoretical analysis and numerical results show that a charged dust cloud immersed in a plasma under the action of electric field and other force, could develop a long-time and steady structures, which can be used to explain the experimental observations, as is shown in Fig. 16.

H. Li, et al., "Study on the sharp boundary of layered dust structure in the summer polar mesopause", Chinese Journal of Polar Research 21(4), 272–278, 2009.

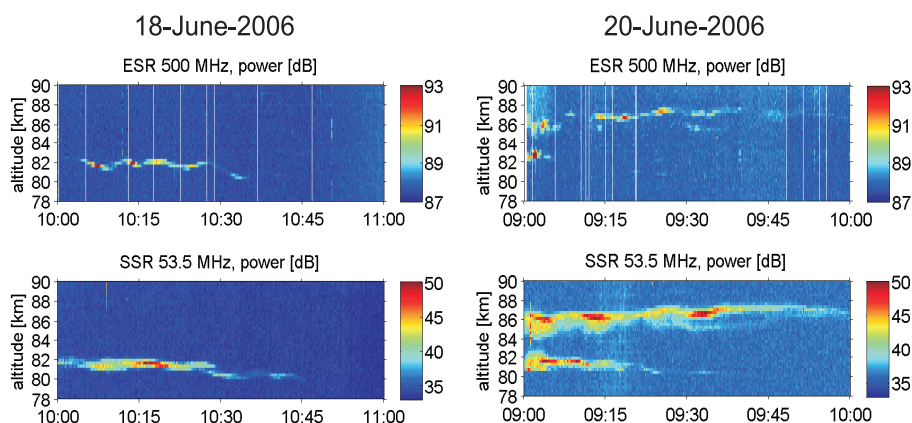


Figure 15: Height-Time-Intensity plots of the radar echoes observed with the ESR at 500 MHz (upper panels) and SSR at 53.5 MHz (lower panels) on 18 June (left column) and 20 June 2006 (right column), respectively. White vertical lines in the upper panels indicate times where meteor echoes were removed.

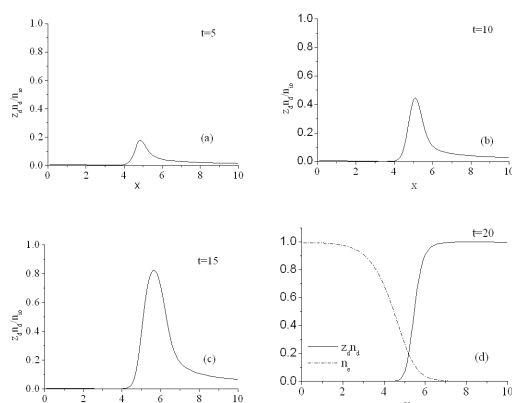


Figure 16: The charged ice particle number density distribution profiles.

Studies involving artificial ionospheric heating

HF heating campaigns by AARI

Two extensive HF heating campaigns were held by Arctic and Antarctic Research Institute in 2009. Russian EISCAT/Heating campaigns were carried out from 3 to 12 March and from 29 October to 6 November 2009. The experiments were carried out in the day and early evening hours in a deep minimum of solar activity under quiet magnetic conditions. Many hours of excellent data were obtained from the EISCAT monostatic UHF radar, the spectrum analyzer for monitoring the SEE frequency spectrum at Tromsø, and the bi-static HF radio scatter at St. Petersburg. Importantly both

campaigns were supported by the Finland and Iceland CUTLASS HF radars. A number of important new results were obtained from these heating campaigns in 2009.

HF pump-induced phenomena near the third electron gyro harmonic frequency, $3f_{ce}$, using the frequency stepping the HF heater frequency, were analysed in detail for a few days of March 2009. As an example, Fig. 17 illustrates the behaviour of the electron temperature T_e and the backscattered power at different operational frequencies from the CUTLASS Finland radar on 9 March 2009 when the heater frequency was changed around the third electron gyro harmonic frequency. The third electron gyro harmonic frequency $3f_{ce}$ was estimated as a frequency on which the disappearance of the DM component in stimulated electromagnetic emission (SEE) spectra occurs. It was found that artificial field-aligned irregularities (AFAIs) with a spatial scale across the magnetic field of 9 m, corresponding the CUTLASS operational frequency of 17 MHz, are depressed at the third electron gyro harmonic in the lesser degree than the AFAIs with larger scale of 13–15 m (CUTLASS operational frequency of 10 and 13 MHz). The T_e changes are not significant at third electron gyro harmonic when the heater frequency f_H is below the critical frequency f_{oF_2} by 0.5–0.7 MHz. The strongest AFAIs were excited above the third electron gyro harmonic by from 20–30 to 50–70 kHz when the SEE spectra exhibit the generation of the nDM and BSS spectral components. A distinctly different phenomena were observed when the heater frequency was near the critical frequency, $f_H \approx 3f_{ce} \approx f_{oF_2}$.

Such situation was realised on 11 March 2009 during heater-on period from 16:00–16:20 UT ($f_H \approx 3f_{ce} \approx f_{UHR} \approx f_{oF_2}$). Upper hybrid resonance altitude of the pump wave was about 220–230 km. In this case extremely strong electron heating (up to 4500 K) and increases in the electron density up to 30–40% were observed. We expect that in this event the strong Langmuir turbulence was excited near the reflection altitude leading the formation of cavities and acceleration of electrons. The combined effect of upper hybrid resonance and gyro resonance at the same altitude under $f_H \approx f_{oF_2}$ gives rise to strong electron heating and excitation of striations, which at the magnetic zenith leads to HF trapping and extension of HF waves to altitudes where they can excite Langmuir turbulence, leading to fluxes of electron accelerated to energies that produce the measurable ionisation.

The generation of HF heater-induced ion upflows from the ionosphere initiated by powerful O-mode HF radio wave, injected towards the magnetic zenith, has been measured on 11 and 12 March 2009. Note that the observed ion upflows were weaker compared with the heater-induced ion upflows during solar activity maximum. Figure 18 illustrates data from the EISCAT UHF radar at Tromsø, showing effects of HF pumping on 11 March 2009. The UHF radar beam pointed towards magnetic zenith. From 16:15 UT the critical frequency f_{oF_2} was near and then below the heater frequency $f_H=4040$ kHz. It was found that the most intense ion upflows accompanied by the strongest electron heating were observed when the HF pump frequency was near the critical frequency of the F_2 layer. In the course of experiment the DMSP F15 satellite was flying above Tromsø. The comparison between EISCAT UHF radar and DMSP satellite observations has been made for heater-on period 15:20–15:40 UT on 11 March 2009 (in collaboration with E. Mishin and C. Roth).

Figure 19 shows variations in the vertical and horizontal (westward) velocities and the ion density along with their trends obtained by averaging over 10 s sliding window. $T_{MZ}=15:26:15$ UT is the time of the shortest distance, about 70 km, from the magnetic zenith of the heater. The oval boundary is about 20 s from T_{MZ} . F17 flew 5° to the west and showed no signatures of heating. Clearly seen near MZ are the ion density enhancement and short-scale oscillations in both velocity components.

It is well known that artificial field-aligned irregularities (AFAIs) are excited near the reflection

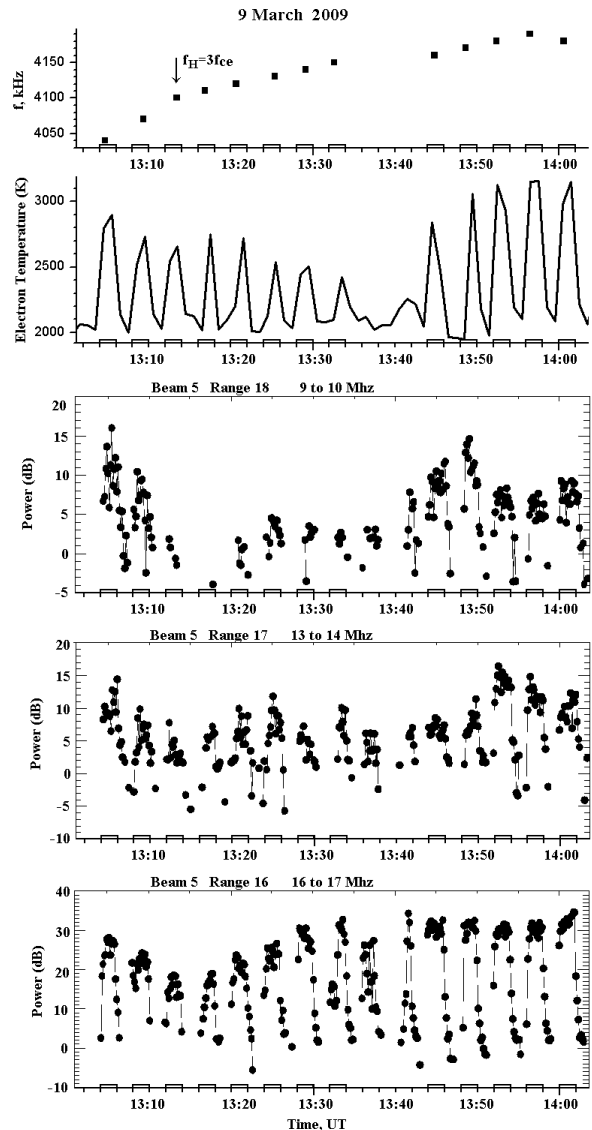


Figure 17: Behaviour of electron temperature T_e from UHF radar and backscattered power at operational frequencies of about 9, 13, and 17 MHz from the CUTLASS Finland radar on 9 March 2009 from 13 to 14:04 UT. The heater frequency was changed by steps from 4040 to 4190 kHz. The heater frequency was very close to the third electron gyro harmonic frequency at 13:12–13:14 UT. Heater-on periods at 13:36–13:38 and 14:08–14:10 UT were aborted and cycles from 13:32, 13:40 had a slow tune (more than 1 min).

level of powerful HF radio wave with O-mode of polarization at the the upper-hybrid resonance (UHR) altitude. Theoretical work undertaken in the 1970s indicated that the thermal parametric instability (Grach and Trakhtengerts, 1976) and resonance instability (Vas'kov and Gurevich, 1976)

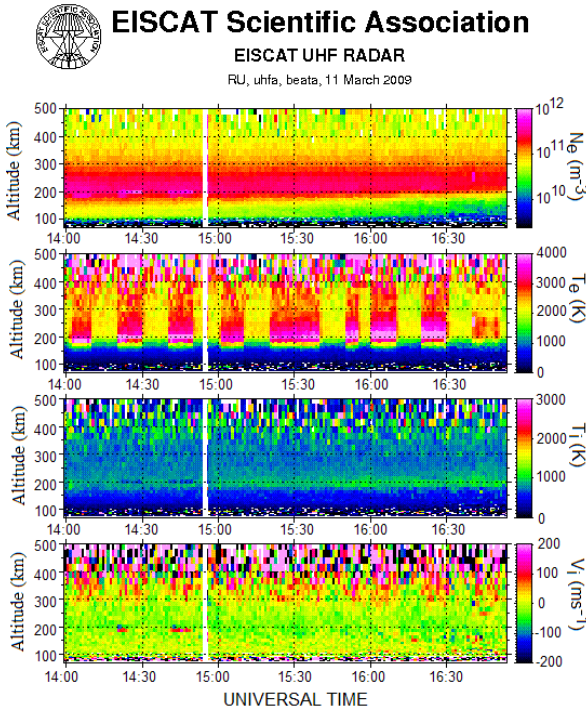


Figure 18: Data from the EISCAT UHF radar at Tromsø, showing effects HF pumping on 11 March 2009. The UHF radar beam pointed towards magnetic zenith.

plays an important role in the generation of such irregularities. The generation of AFAIs is not possible for a powerful HF radio wave with X-mode polarisation. The reason is that such HF wave is reflected below from the UHR height and AFAIs can not be excited. During the October-November 2009 campaign for the first time very strong AFAIs were detected with unusual features when HF pumping was produced at X-mode polarisation and the heater frequency f_H significantly exceeded f_{oF_2} . A comparison between backscattered signals observed from CUTLASS radars and bi-static HF radio scatter observations in St. Petersburg has been made (in collaboration with T. Yeoman). Figures 20 and 21 depict CUTLASS Hankasalmi radar data obtained on 5 and 6 November 2009.

From Figs. 20 and 21 it can be seen that the change of the HF pump wave polarisation from O-mode to X-mode leads to the appearance of strong backscattered signals. HF pumping was produced at frequency of 4040 kHz. The critical frequency of ordinary mode from ionosonde data was about 3.2 MHz. It is important to note that strong backscattered signals under X-mode polarisation of HF pump wave appeared when f_H was comparable with f_{xF_2} . The signals scattered from

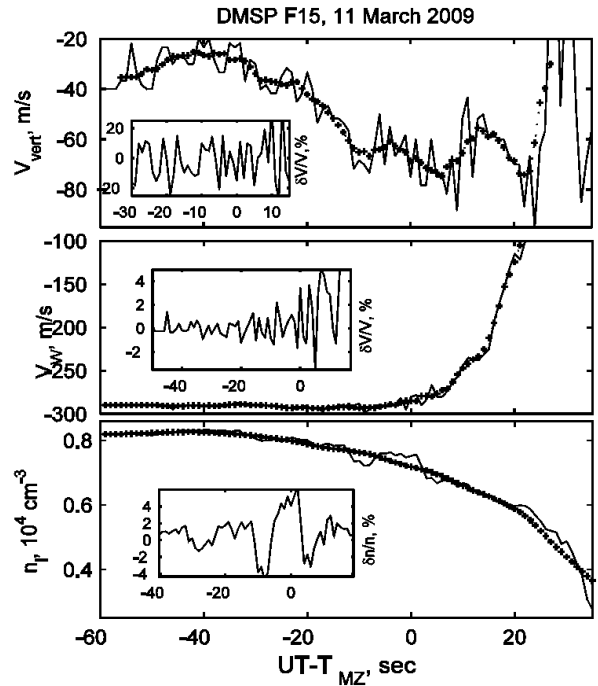


Figure 19: Variations in the vertical and horizontal (westward) velocities and the ion density along with their trends obtained at the DMSP F15 satellite on 11 March 2009. Insets show the detrended values. The shortest distance, about 70 km, from the magnetic zenith of the heater was observed at $T_{MZ}=15:26:15$ UT.

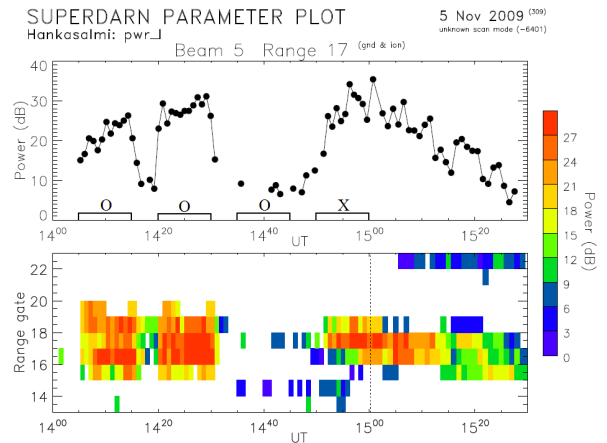


Figure 20: Backscattered power from CUTLASS Hankasalmi radar at operational frequency of about 10 MHz in the 18 range gate (top panel) and in range gates from 13 to 23 (bottom panel) on 5 November 2009.

heater-induced irregularities did not disappear after the heater was turned off. In addition, the temporal decay of heater-induced irregularities, seen in CUTLASS beam 5 backscatter, is unusually long

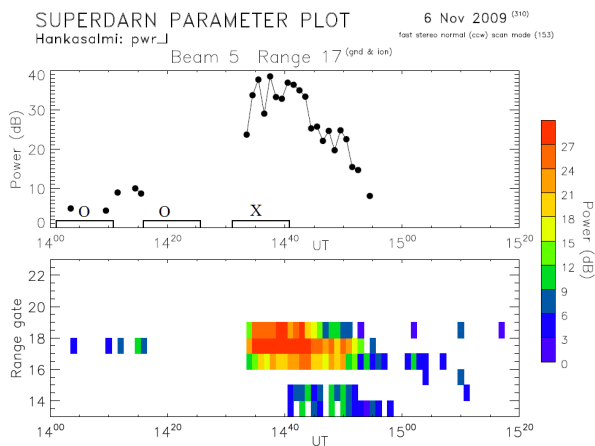


Figure 21: Backscattered power from CUTLASS Hankasalmi radar at operational frequency of about 10 MHz in the 18 range gate (top panel) and in range gates from 13 to 23 (bottom panel) on 6 November 2009.

and ranges up to 30 minutes. In the course of experiments the UHF radar was running at Tromsø. Data from the UHF radar showed some increase in electron temperatures in the comparison with O-mode heating at frequencies far above the f_{oF_2} . The physical justification of the observed new phenomenon is not well-understood at present. There is a need to continue studies in this area by using a variety of techniques and methods to provide the formulation of a clear theoretical picture of high power HF ionospheric interactions.

N. F. Blagoveshchenskaya, et al., "Phenomena induced by powerful HF pumping towards magnetic zenith with a frequency near the F-region critical frequency and the third electron gyro harmonic frequency", *Annales Geophysicae* 27(1), 131–145, 2009.

N. F. Blagoveshchenskaya, et al., "SPEAR-induced field-aligned irregularities observed from bi-static HF radio scattering in the polar ionosphere", *Journal of Atmospheric and Solar-Terrestrial Physics* 71(1), 11–20, 2009.

T. D. Borisova, et al., "Peculiarities of stimulated electromagnetic emission under action of higher-power HF radiowaves, emitted by the SPEAR facility, on the sporadic E layer of the polar ionosphere", *Geomagnetism and Aeronomy* 49(5), 653–663, 2009. *ERRATA: Geomagnetism and Aeronomy*, 49(6), 822, 2009.

T. D. Borisova, et al., "Splitting of the Doppler frequency shift of bi-static backscatter signals during the Sura experiments", *Geomagnetism and Aeronomy* 49(4), 510–518, 2009.

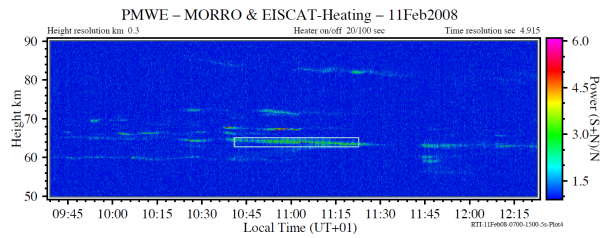


Figure 22: The PMWE layer used in the analysis.

A. V. Zalizovski, et al., "Self-scattering of a powerful HF radio wave on stimulated ionospheric turbulence", *Radio Science* 44, RS3010, doi:10.1029/2008RS004111, 2009.

Artificial modification of polar mesospheric winter echoes with the EISCAT Heater and the role of charged dust particles

An investigation of polar mesosphere winter echoes (PMWE) has been carried out with the mesosphere-stratosphere-troposphere Mobile Rocket and Radar Observatory (MST MORRO) radar operating at 56 MHz. MORRO has been deployed at the European Incoherent Scatter (EISCAT) installation near Tromsø in northern Norway, co-located with the EISCAT's VHF and UHF radars and RF heating facility. The main object of the investigation is to examine whether, and if so, how, RF heating influences PMWE. In particular, an experimental confirmation of the overshoot effect would indicate the presence of charged dust particles. On 11 February 2008 we measured several weak and variable PMWE layers and we used the RF heater with an on period of 20 s and off period of 100 s to modulate the radar scatter from the layers. We chose one layer, which for 44 min was the strongest and most stable layer, for further analysis; see Fig. 22 where the layer in question is framed.

The signal intensity variation during an averaged on/off heater period shows the expected weakening of the signal intensity when heating is turned on, followed by a significant small recovery of the signal during the on phase and a corresponding small overshoot of the signal strength of about 13–15% over the background level when heating is switched off, see Fig. 23. The recovery and overshoot are attributable to charge accumulation on the dust particles due to electron heating. The overshoot characteristic curve shows that a considerable increase in the electron temperature

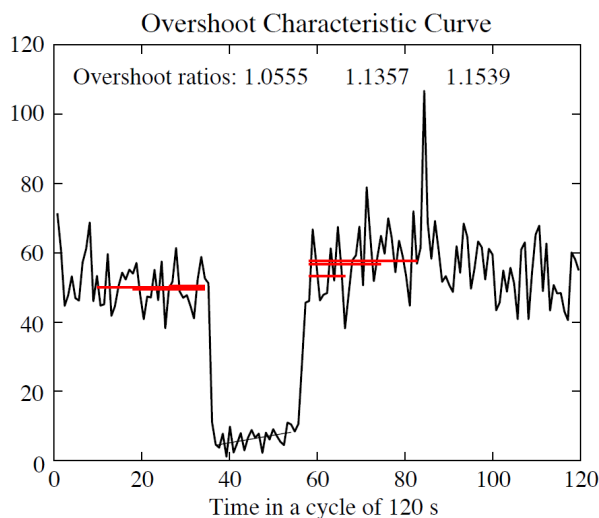


Figure 23: Characteristics of the signal strength during an on/off heater period.

did take place during heating and that charged dust particles should be present, probably with a radii of some nanometers.

C. La Hoz and O. Havnes, "Artificial modification of polar mesospheric winter echoes with an RF heater: Do charged dust particles play an active role?", *Journal of Geophysical Research* 113, D19205, doi:10.1029/2008JD010460, 2008.

Polar ionospheric heating

By analysing ISR observation data, the heating effects in polar winter ionospheric modification experiments carried out in January 2008 at Tromsø, Norway, were studied. A clear disturbance effect is present under the O-mode over-dense heating conditions. The enhancement of the electron temperature is up to 60%–120%, extending from 150 km to 400 km. The disturbance of the electron density is not obvious, with a 12% maximum decrease. A 1–2 kHz increase in the acoustic frequency can be observed, an enhancement in the peak-to-valley ratio of the ion line and sometimes its high-order harmonics can be seen as well. The power of the ion line and plasma line has shown overshoot effect, single-humped, double-humped and triple-humped structures have appeared in the power profile of plasma line, and the enhancement in power amplitude of the plasma line decreases exponentially as the frequency increases.

Additionally, with consideration of the elastic collision between electrons and neutral particles and the excitation of rotation energy level, the effects of ionospheric heating on the spectra are in-

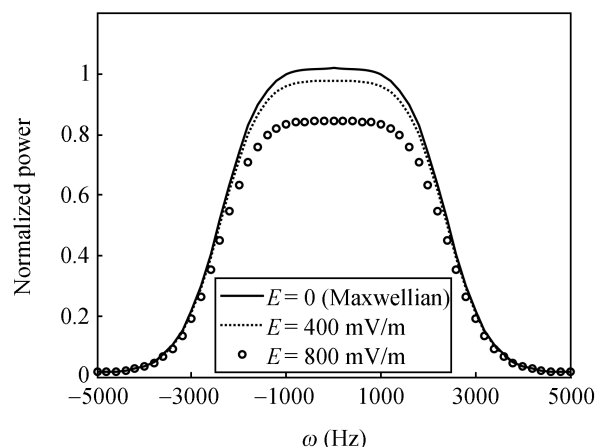


Figure 24: Spectra with electric field.

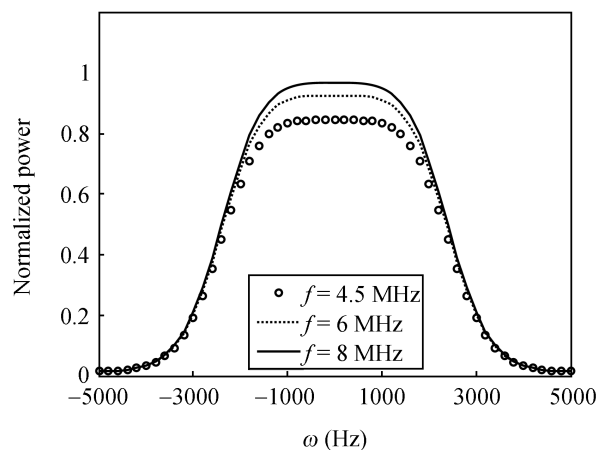


Figure 25: Spectra with pump frequency.

vestigated. Results show that with the increase in electric field, the non-Maxwellian feature is enhanced as indicated by Fig. 24. Figure 25 shows that the non-Maxwellian feature is weakened as the increase in heating frequency.

B. Xu, et al., "Incoherent scatter spectra due to HF heating in the low ionosphere region, *Science in China Series E (Technical Sciences)* 52(2), 1–5, 2009.

B. Xu, et al., "Observations of the heating experiments in the polar winter ionosphere", *Chinese Journal of Geophysics* 52(4), 859–877, 2009.

F-region electron heating by X-mode radiowaves

Modifications of the electron temperature in the F-region produced by powerful high frequency radiowaves at 4.04 MHz transmitted in X-mode were observed (Fig. 26). The experiments were

performed during quiet nighttime conditions with low ionospheric densities so no reflections occurred. Electron temperature enhancements of the order of 300–400 K were obtained. Numerical simulation of ohmic heating by the pump wave reproduces both altitude profiles and temporal dependence of the temperature modifications in the experiments.

H. Löfås, et al., "F-region electron heating by X-mode radiowaves in underdense conditions, *Annales Geophysicae* 27(6), 2585–2592, 2009.

Ionospheric modification and plasma physics

The Space Plasma Exploration by Active Radar (SPEAR) facility, co-located with ESR, has been used to study aspect sensitive phenomena when the ionosphere is pumped with HF radio waves. Observations of E- and F-region SPEAR-induced spectral enhancements consistent with the actions of both the purely growing mode and the parametric decay instability, together with E-region enhancements consistent with mode conversion along sporadic E-layer vertical gradients near the critical layer have been made (Fig. 27). Consistent enhancements from field-aligned, around vertical and also from 5° south of field-aligned were found. Reasons for the prevalence of observations from (close to) vertical include the existence of the Spitzø region, throughout which propagating high-power waves may reach their highest possible reflection point where RF-induced instabilities may be excited. In addition, observations of enhanced field-aligned scatter may be aided by the presence of field-aligned irregularities, which may guide the electrostatic waves that are excited by RF-induced instabilities. However, the enhancements for pointing directions of ~5–8° south of field-aligned require further investigation.

The first power-stepping experiments using SPEAR have been performed. Both CUTLASS SuperDARN radars detected backscatter from SPEAR-induced Artificial Field-Aligned Irregularities (AFAIs) while the effective radiated power of SPEAR was varied from 1–10 MW. It was demonstrated that AFAI could be excited by a SPEAR ERP of only 1 MW and that once created the irregularities could be maintained for even lower powers. The experiment also demonstrated that the very high latitude ionosphere exhibits hysteresis, where the down-going part of the power cycle provided a higher density of irregularities than for the equivalent part of the up-going cycle. The ESR

ESR BACKSCATTER DATA

F-CIL, E-CIL, UPL and DPL on 07/12/2005

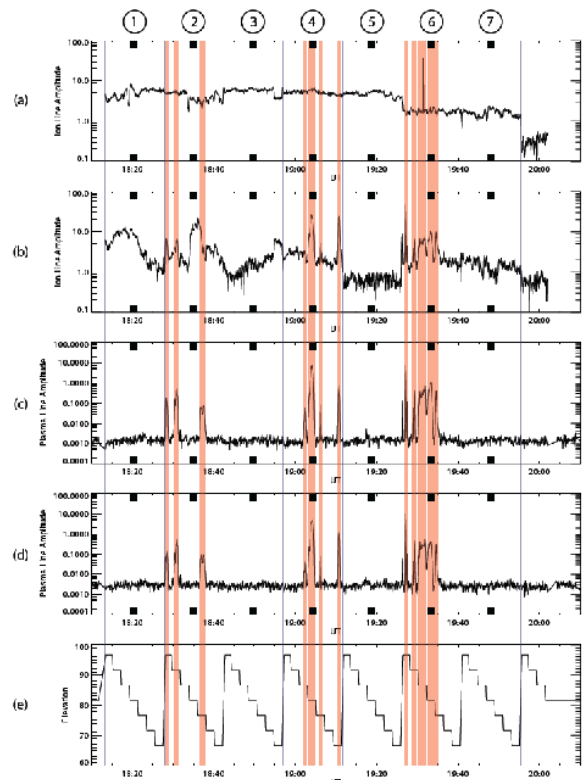


Figure 27: ESR ion and plasma line amplitudes from 7 December 2005. Panels (a) to (d) show the F-region ion-line (150–250 km), E-region ion-line (80–110 km), the upshifted plasma-line and downshifted plasma-line, respectively. Panel (e) shows the 32 m dish elevation angle. ESR field-aligned (FA) pointing is denoted by black rectangles. The red bars indicate periods of high ion or plasma line amplitude consistent with the action of SPEAR. There are clear ion and plasma line spectral enhancements from several directions, including from FA+15°, FA+10°, FA+5°, FA, FA-5° and FA-15°, with notable enhancement occurring in FA. The upshifted and downshifted plasma line enhancements occur mainly in the E-region and are clearly well correlated, both with each other and with the ion line enhancements.

failed to detect any hysteresis in the plasma parameters over Svalbard in stark contrast with previous UHF measurements.

SPEAR has also been employed to excite ULF waves on local magnetic field lines. An interval from February 2006, when SPEAR was transmitting a 1 Hz modulation signal with a 10 min on/off cycle was investigated. Ground magnetometer data indicated that SPEAR modulated currents in

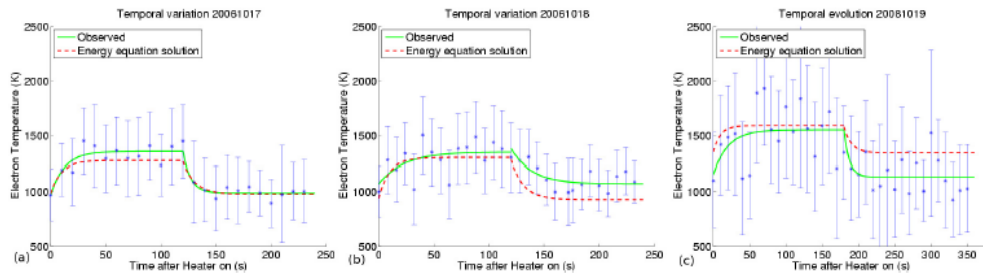


Figure 26: Temporal evolution of the electron temperature for the three different days, (a) 17 October, (b) 18 October and (c) 19 October. Temperatures derived from conditionally averaged raw radar data, received at the same offset time from the nearest HF on time, are plotted vs time along with the error bars. Exponential fits to temperature rise and fall are shown in green. Results of the time dependent modeling of collisional ohmic heating by the pump wave are shown in red.

the local ionosphere at 1 Hz, and enhanced a natural field line resonance with a 10 min period. Overhead signatures of the SPEAR-enhanced field line resonance were present in the magnetic field data measured by the magnetometer on-board Cluster 2. These results were the first joint ground- and space-based detections of field line tagging by SPEAR.

R. S. Dhillon, T. R. Robinson, and T. K. Yeoman, “Aspect sensitive E- and F-region SPEAR-enhanced incoherent backscatter observed by the EISCAT Svalbard radar”, *Annales Geophysicae* 27(1), 65–81, 2009.

D. M. Wright, et al., “Excitation thresholds of field-aligned irregularities and associated ionospheric hysteresis at very high latitudes observed using SPEAR-induced HF radar backscatter”, *Annales Geophysicae* 27(7), 2623–2631, 2009.

S. V. Badman, et al., “Cluster spacecraft observations of a ULF wave enhanced by Space Plasma Exploration by Active Radar (SPEAR)”, *Annales Geophysicae* 27(9), 3591–3599, 2009.

Studies of the thermosphere

Temperature enhancements and vertical winds in the lower thermosphere associated with auroral heating during the Dynamics and Energetics of the Lower Thermosphere in Aurora (DELTA) campaign

A coordinated observation of the atmospheric response to auroral energy input in the polar lower thermosphere was conducted during the Dynamics and Energetics of the Lower Thermosphere in

Aurora (DELTA) campaign. N_2 rotational temperature was measured with a rocket-borne instrument launched from the Andøya Rocket Range, neutral winds were measured from auroral emissions at 557.7 nm with a Fabry-Perot Interferometer (FPI) at Skibotn and the KEOPS, and ionospheric parameters were measured with the European Incoherent Scatter (EISCAT) UHF radar at Tromsø. Altitude profiles of the passive energy deposition rate and the particle heating rate were estimated using data taken with the EISCAT radar. The local temperature enhancement derived from the difference between the observed N_2 rotational temperature and the MSISE-90 model neutral temperature were 70–140 K at 110–140 km altitude. The temperature increase rate derived from the estimated heating rates, however, cannot account for the temperature enhancement below 120 km, even considering the contribution of the neutral density to the estimated heating rate. The observed upward winds up to 40 m/s seem to respond nearly instantaneously to changes in the heating rates (see Fig. 28). Although the wind speeds cannot be explained by the estimated heating rate and the thermal expansion hypothesis, the present study suggests that the generation mechanism of the large vertical winds must be responsible for the fast response of the vertical wind to the heating event.

J. Kurihara, et al., “Temperature enhancements and vertical winds in the lower thermosphere associated with auroral heating during the Dynamics and Energetics of the Lower Thermosphere in Aurora (DELTA) campaign”, *Journal of Geophysical Research* 114, A12306, doi:10.1029/2009JA014392, 2009.

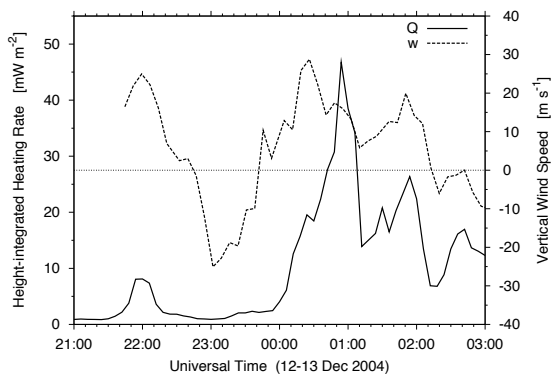


Figure 28: Time variations of the height-integrated heating rate derived from the data observed with the EISCAT UHF radar at Tromsø (solid line) and vertical wind speed derived from the auroral green line observation with the Fabry-Perot Interferometer at Skibotn (dashed line).

Meso-scale thermospheric response

The meso-scale response of the thermosphere has been studied at ESR on 5 Dec 2007 in conjunction with the Svalbard Fabry-Perot Interferometer (FPI) and SCANNing Doppler Imager (SCANDI) for a very localised heating event, in both time and space, corresponding to the IMF B_z going negative for ~ 50 minutes. Both optical instruments measure neutral wind velocity and temperature, which began to respond within 15 minutes to the onset of the disturbance. This is far more rapid than expected. The localised winds were accelerated by up to 100 m/s over a period of half an hour while the winds in the rest of the region were fairly steady. The neutral temperature rose by ~ 100 K over a period of 40 minutes over the entire field of view. The importance of these observations is that significant meso-scale variability is present in the thermosphere and therefore needs to be incorporated into models in order to properly account for energy dissipation in the thermosphere.

E. M. Griffin, et al., "Upper thermospheric ion-neutral coupling from combined optical and radar experiments over Svalbard", *Annales Geophysicae* 27(11), 4293–4303, 2009.

Acceleration mechanism of high-speed neutral wind observed in the polar lower thermosphere

We investigated the acceleration mechanism of the lower thermospheric neutral wind when the iono-

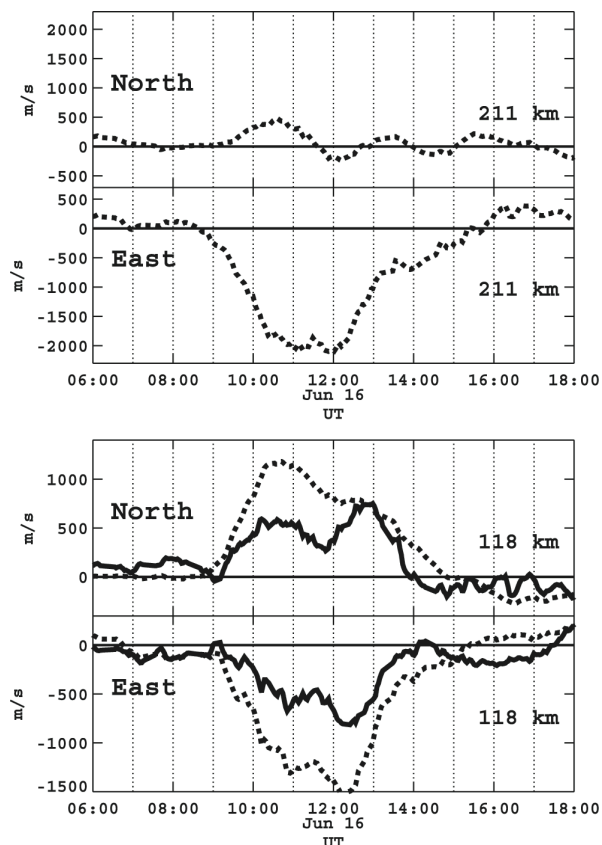


Figure 29: The ion velocity at 211 km and (bottom) ion (dotted line) and neutral wind (solid line) velocities at 118 km observed from 0600 to 1800 UT on 16 June 2005 with ESR.

spheric convection becomes enhanced. The ESR CP2 measurement on 16 June 2005 detected that the lower thermospheric wind accelerated to unusually high speed (~ 500 m/s) (Fig. 29). This wind acceleration seemed to be well corresponding with the enhanced ionospheric convection after changes of the solar wind parameters by the ACE satellite. We evaluated the ion drag and the Joule-heating-induced pressure gradient contributions on the generation of the high-speed neutral wind. We concluded that the pressure gradient force was the most probable force in this event.

T. T. Tsuda, et al., "Acceleration mechanism of high-speed neutral wind observed in the polar lower thermosphere", *Journal of Geophysical Research* 114, A04322, doi:10.1029/2008JA013867, 2009.

DELTA-2 campaign: Study of the energetics and the wind dynamics in the polar lower thermosphere

Dynamics and Energetics of the Lower Thermosphere in Aurora 2 (DELTA-2) campaign was conducted under collaboration with the rocket, the EISCAT UHF radar, Fabry-Perot interferometer (FPI), and various optical instruments in order to study the energetics and the wind dynamics in the polar lower thermosphere from January 14 to 26, 2009. The S-310-39 sounding rocket, which carried trimethyl aluminum (TMA) to conduct in-situ measurement of the neutral wind, was launched from the Andøya rocket range at 00:15 UT on 26 January 2009. An auroral breakup occurred about 10 minutes from the rocket launch. The EISCAT UHF radar was operated for 107.5 hours during the campaign under international collaborations with Norway, Sweden, Finland, Germany, France, and Japan. The data set taken during the campaign is appropriate for studying many scientific issues such as the wind dynamics, ionospheric conductivity, and current system. FPI (557.7 nm) was operated with the rocket observation, and it provided dramatic wind variations associated with the breakup.

Studies of dust and meteorites

Measurements of meteor smoke particles during the ECOMA-2006 campaign

The EISCAT (European Incoherent SCATter) radars did support the ECOMA (Existence and Charge state Of Meteoric smoke particles in the middle Atmosphere) campaign conducted at Andenes (Andøya Island, Norway, 69°N, 16°E) in 2006. Instrumented rockets were launched to investigate meteoric smoke particles. These particles play an important role in atmospheric processes such as in the nucleation of noctilucent clouds (NLC) and polar stratospheric clouds (PSC). The experimental quantification of these meteor smoke particles is a highly challenging and ongoing scientific project using in-situ rocket and ground-based radar observations. A new rocket-borne particle detector which is a combination between a classical Faraday cup and a Xenon flashlamp for active photoionisation of meteoric dust particles and their subsequent detection of corresponding photoelectrons was introduced by Rapp and Strelnikova (2009). The first rocket during the ECOMA-2006 campaign was further equipped

with instruments to measure several plasma parameters during the flight at mesospheric altitudes. A detailed analysis of the results of the ECOMA-01 rocket launch was published by Strelnikova et al. (2009) which clearly describes the instrumentation of the rocket payload and the scientific results.

In the following, one experiment on ECOMA-01 will be presented in more detail. Onboard the ECOMA payload a radio wave propagation experiment was launched to measure electron densities using the differential absorption of radio waves. The neutral and ionised background atmosphere was simultaneously observed by the EISCAT radars located near Tromsø, Norway. During the night of the rocket launch the EISCAT radars detected an enhanced ionization in the D-region created after an energetic partial precipitation starting at 21:58 UT on Sep. 8, 2006. Shortly after this time a sporadic E-layer (E_s) developed with maximum electron number densities of $\sim 10^5 \text{ cm}^{-3}$ at an altitude of 94.5 km. The layer was quite stable for about an hour and settled down until it disappeared around 0:00 UT. The electron densities were observed with both EISCAT radars on the mainland (VHF and UHF). Fig. 30 shows the electron density measurements obtained from the EISCAT UHF radar around the launch time of the rocket which is indicated by the vertical line. The ionospheric conditions were moderate to quiet which was also confirmed by riometer measurements. The right hand panel shows the electron densities obtained from both, UHF and VHF, radars and the radio wave propagation experiment. Between 93 and 96 km an increase of electron number densities was observed where the red line shows the results from the Faraday rotation experiment. Note that the altitude difference of the sporadic E-layer might be due to the horizontal distance between the radar sites and the rocket location (~ 130 km). Comparing ground-based and in-situ experimental results of electron number density measurements leads to qualitatively and quantitatively similar results.

Simultaneously, temperatures measurements were obtained from the colocated Na-lidar and the RMR-lidar as well as from the rocket-borne neutral air density measurements. These measurements show temperatures in large excess of the frost point of water indicating that ice particles could not be formed at mesospheric altitudes at the time of the in-situ rocket measurements (Strelnikova et al., 2009). On the other hand, the ECOMA detector registered particle signatures in both data chan-

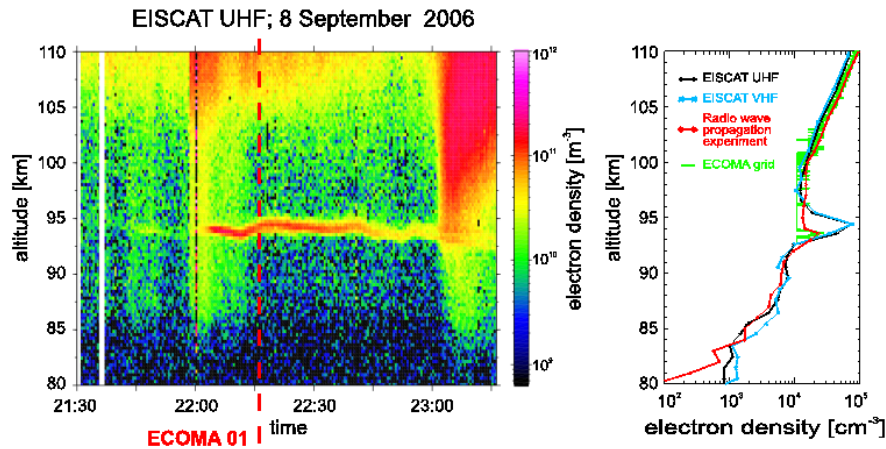


Figure 30: Left panel: Electron number densities measured with the EISCAT UHF-radar on 8 September 2006. The red vertical line indicates the time of the ECOMA-01 start. Right panel: Electron number density profile from the EISCAT UHF and VHF radars (black and blue lines) from the time of the ECOMA-01 launch compared to the in situ results from the Faraday rotation experiment (red line) and the current to the positively biased front grid of the ECOMA particle detector (green line, normalized to the Faraday rotation experiment at 110 km altitude). Note that the difference in altitude of the sporadic layer seen in the radar and rocket measurements is likely due to the horizontal distance between the different observations (~ 130 km).

nels, the directly impacted particles on the detector electrode and the photoelectrons generated by photoionisation or photodetachment of particles. These photoelectron measurements showed that particles exist in the entire altitude range between 60 and 90 km. The measured currents were converted to meteor smoke particle number densities which are in qualitative agreement with model predictions.

M. Rapp, and I. Strelnikova, “Measurements of meteor smoke particles during the ECOMA-2006 campaign: 1. Particle detection by active photoionization”, *Journal of Atmospheric and Solar-Terrestrial Physics* 71(3–4), 477–485, doi:10.1016/j.jastp.2008.07.011, 2009.

I. Strelnikova, et al., “Measurements of meteor smoke particles during the ECOMA-2006 campaign: 2. Results”, *Journal of Atmospheric and Solar-Terrestrial Physics* 71(3–4), 486–496, doi:10.1016/j.jastp.2008.07.011, 2009.

High statistics radar meteor studies at EISCAT

An experiment was conducted with the European Incoherent Scatter (EISCAT) radars during three 8-hour runs on consecutive nights in December 2008 aiming to detect and study the high-altitude meteor population along with the meteors detected at

classical ~ 100 km altitudes. The experiment used coaxial ultrahigh-frequency (UHF) and very high-frequency (VHF) radar beams pointed vertically to the zenith of Ramfjordmoen near Tromsø (Norway), and remote UHF receivers at Kiruna (Sweden) and Sodankylä (Finland) for tristatic observations of a very limited volume at an altitude of 170 km above the transmitter site.

The EISCAT VHF radar detected during the 24-hour period 22,698 echoes identified as meteors. The number of UHF echoes in the same period was 2138, most detected also at VHF. Among the VHF meteors, 11 were detected at altitudes higher than 150 km. Of these, the record highest meteor was at 246.9 km. No high-altitude UHF echoes were detected, none was tristatic, and no echoes with a Doppler velocity above ~ 60 km/s were identified. Given the large number of echoes, which argues in favour of a highly significant characterization of the meteoroid population, we discuss the statistical properties of the detections and their possible physical nature.

The average detection rate of VHF radar meteors was about 16 min^{-1} . Comparing this high rate with that of the faintest optically detected meteors indicates that the radar detections originate from a meteoroid population that could be as optically faint as 13–14 mag. We did not observe a marked enhancement of the rates at the peak of the Gem-

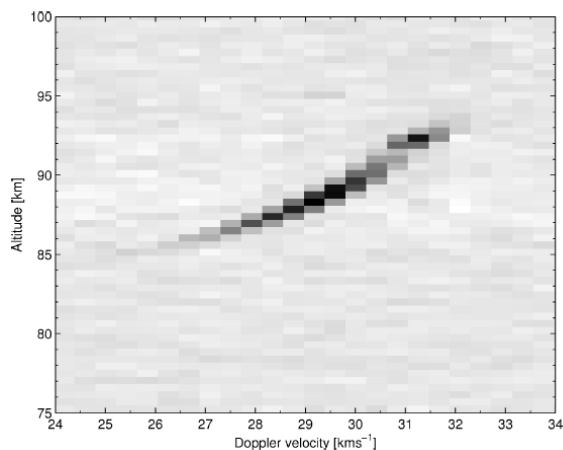


Figure 31: Altitude–Doppler-intensity plot for one meteor track. The deceleration is evident since the Doppler velocity is smaller at lower altitudes. The visible curvature of this plot implies that the deceleration was not constant; the meteoroid decelerated faster at lower altitudes.

inid shower, confirming once again the proposal that most faint meteors, be these radar or optical, belong to the sporadic population and not to a specific shower.

For a few meteors, our data show definite deceleration and possible fragmentation (Fig. 31). A simple calculation indicates that one of the detected meteoroids was a submillimetre body that fragmented when the ram pressure reached about 0.5 Pa. This is much lower than the pressure that fragments brighter cometary meteors, which is at least two orders of magnitude higher.

N. Brosch, et al., “Unusual features in high statistics radar meteor studies at EISCAT”, *Monthly Notices of the Royal Astronomical Society* 401(2), 1069–1079, 2010.

Signatures of mesospheric particles in ionospheric data

During a ECOMA/MASS campaign in 2007, three sounding rockets were launched from Andøya, Norway. This campaign was supported by several ground-based observations including the EISCAT UHF and VHF radars near Tromsø. The electron density measurements from the EISCAT UHF radar were considered in the discussion by Friedrich et al. (2009). In the ionospheric E-region the agreement between the EISCAT UHF and the in-situ probing of electron densities is remarkably good. It is well known that below 90 km the ground-based radar data reflect the coherent

backscatter due to the occurrence of polar mesosphere summer echoes (PMSE) rather than electron densities. The interpretation of the radar backscatter for altitudes below 90 km is based on the physics of PMSE.

M. Friedrich, et al., “Signatures of mesospheric particles in ionospheric data”, *Annales Geophysicae* 27(2), 823–829, 2009.

Solar wind studies

Interaction a between medium-scale transient in the solar wind and a stream interaction region

We have combined Inter-Planetary Scintillation (IPS) measurements from EISCAT with white-light observations from the STEREO spacecraft HI instrument to study the interaction a between medium-scale transient in the solar wind and a stream interaction region, showing the transient started within the slow wind and was subsequently captured by the star interaction region. We have also observed smaller scale transients in the slow wind, associated with significant field rotations. It is not yet clear whether these features are ubiquitous in the slow wind or associated with Coronal Mass Ejection (CME) wakes, but they might be the same class of structures as the pixel-scale features seen in LASCO spacecraft observations of the slow wind. An associated study combined EISCAT and STEREO HI solar wind observations with in-situ measurements from Venus Express ASPERA-4 instrument to study the impact of stream interaction regions and solar wind transients on the Venus environment.

The large-scale structure in the solar wind has been investigated using IPS. EISCAT data played a key role in improving understanding of the evolution of the large CME of May 2005. A programme of comparing EISCAT IPS and STEREO white-light results with the predicted signatures derived from a multi-scale numerical model is underway, simulating IPS and white-light scattering by a CME, interacting CMEs or CME/stream interaction region structures as they propagate through the background solar wind. This development will significantly improve our ability to determine precisely which region of a CME the EISCAT observations correspond to.

G. D. Dorrian, et al., “Transient structures and stream interaction regions in the solar wind: Results from EISCAT interplanetary scintillation, STEREO HI and Venus

Express ASPERA-4 observations”, *Solar Physics*, submitted, 2010.

I. C. Whittaker, et al., “In-situ observations of a co-rotating interaction region at Venus identified by IPS and STEREO”, *Solar Physics*, in press, 2010.

M. M. Bisi, et al., “Three-dimensional reconstructions of EISCAT IPS velocity data during the declining phase of solar cycle 23”, *Solar Physics*, in press, 2010.

M. M. Bisi, et al., “From the Sun to the Earth: the 13 May 2005 Coronal Mass Ejection”, *Solar Physics*, submitted, 2010.

M. Xiong, et al., “Forward modelling to determine the observational signatures of white-light imaging and interplanetary scintillation for the propagation of an interplanetary shock in the ecliptic plane”, *Journal of Atmospheric and Solar Terrestrial Physics*, submitted, 2010.

Theoretical studies of incoherent scattering spectra

20-moment approximation for ion velocity distribution and its application in calculations of incoherent scatter spectra

According to Grad’s theory, the ion velocity distribution function is expanded about a 20-moment approximation based on Maxwellian distribution. The effects of the stress tensor and the heat flow vector on the ion velocity distributions are discussed. When the electric field is weak, it is reasonable to neglect the heat flow vector and the stress tensor parallel to $\mathbf{E} \times \mathbf{B}$ and \mathbf{E} , respectively. The ion temperature anisotropy and asymmetry in the distribution function are caused by the stress tensor and the heat flow term. The incoherent scatter spectra calculated by the 13-moment approximation and the 20-moment approximation are compared. When the electric field is weak, the 13-moment is nearly consistent with the 20-moment approximation. However it is unreasonable to neglect the heat flow tensor, and the temperature anisotropy is distinct in case of strong electric field as is seen in Fig. 32). It is reasonable to use the 20-moment approximation to describe the non-Maxwellian plasma characterized by the temperature anisotropy.

In addition, a sixteen moment approximation based on a bi-Maxwellian that contains the stress tensor and the heat flow vector is applied to describe the ion velocity distribution which is suitable for the non-Maxwellian plasma characterised

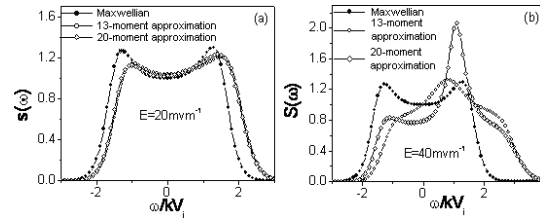


Figure 32: The 20-moment approximation for the incoherent scattering spectra parallel to $\mathbf{E} \times \mathbf{B}$ for different electric field \mathbf{E} .

by the large temperature anisotropy. A discussion is made about the effects on the incoherent scatter spectra caused by different values of the normalized perpendicular drift velocity \mathbf{D} , aspect angle ϕ between the magnetic field and the line-of-sight direction, and the ratio α of the ion-neutral collision to ion cyclotron frequency. Numerical results show that the shifting and asymmetry of incoherent scatter spectra appear parallel to $\mathbf{E} \times \mathbf{B}$ and \mathbf{E} as the normalised perpendicular drift velocity \mathbf{D} increases due to the ion drift velocity, the stress tensor and the heat flow vector respectively. However, the spectrum is always typically double-humped Maxwellian parallel to \mathbf{B} . The ion velocity distribution is more distorted from the Maxwellian as the aspect angle ϕ increases from 0° to 90° , and consequently the incoherent scatter spectra is no longer typically double-humped Maxwellian. As α increases, the ion velocity distribution becomes Maxwellian and the incoherent scatter spectra become typically double-humped Maxwellian even with a large value of the normalised perpendicular drift velocity \mathbf{D} .

K. Xue, et al., “20-moment approximation for ion velocity distribution and its application in calculations of incoherent scattering spectra”, *Chinese Journal of Geophysics* 52(2), 342–351, 2009.

K. Xue, et al., “16-moment approximation for ion velocity distribution and its application in calculations of incoherent scattering spectra”, *Plasma Science and Technology* 11(2), 152–158, 2009.

K. Xue, et al., “The ion distribution function from Maxwell molecule collision model and calculations of incoherent scatter spectra”, *Chinese Journal of Space Science* 29(3), 287–295, 2009.

Incoherent scatter spectra of collisional plasma

Incoherent scatter spectra of a collisional plasma with an arbitrary velocity distribution function is

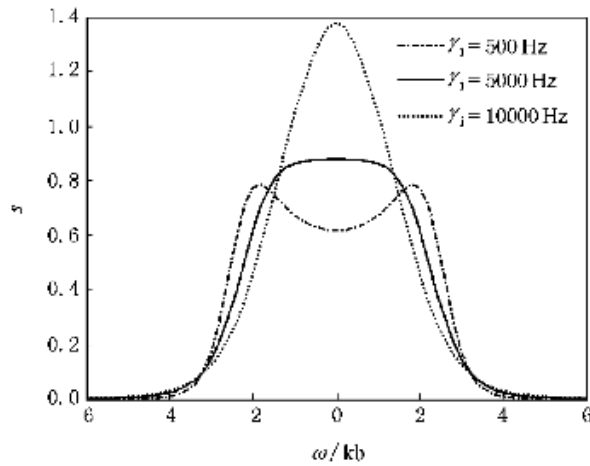


Figure 33: Variation of the power spectrum with different collision frequency.

presented. Two integrals with complex singular points have been solved in order to obtain the results. The incoherent scatter spectra during HF heating in low ionosphere region are computed. A super-Gaussian function is adopted in the calculation with a non-Maxwellian factor m . The effect of collision frequency, non-Maxwellian factor, electron density, electron temperature and ion temperature on power spectra is discussed (Fig. 33). Under the action of collision frequency and non-Maxwellian factor, the original relationship between ionospheric parameters and the characteristics of spectra shape is invalid, which will bring a large error in the inversion of ionosphere parameters, thus the original theoretical model must be corrected.

B. Xu, et al., "Incoherent scatter spectra of a collisional plasma", *Acta Physica Sinica* 58(7), 736–742, 2009.

List of publications 2009

- Aikio, A.T., and A. Selkälä, Statistical properties of Joule heating rate, electric field and conductances at high latitudes, *Ann. Geophys.*, 27, 2661-2673, 2009.
- Blagoveshchenskaya, N.F., H.C. Carlson, V.A. Kornienko, T.D. Borisova, M.T. Rietveld, T.K. Yeoman, and A. Brekke, Phenomena induced by powerful HF pumping towards magnetic zenith with a frequency near the F-region critical frequency and the third electron gyro harmonic frequency, *Ann. Geophys.*, 27, 131-145, 2009.
- Cai, H.T., McCrea I.W., Dunlop M.W., Davies J.A., Bogdanova Y.V., Pitout F., Milan S.E., Lockwood M. and Ma S.Y., Cusp observations during a series of fast IMF Bz reversals., *Ann. Geophys.*, 27, 2721-2737, 2009.
- Cai H.T., Ma S.Y., McCrea I.W., et al., Polar ionospheric responses to 4-times rapid turnings of the IMF Bz component-EISCAT/ESR radar observations, *Chinese J. Geophys.* (in Chinese), 52(7): 1685-1692, 2009.
- Dhillon, R.S., T.R. Robinson, and T.K. Yeoman, Aspect sensitive E- and F-region SPEAR-enhanced incoherent backscatter observed by the EISCAT Svalbard radar, *Ann. Geophys.*, 27, 65-81, 2009.
- Friedrich, M., K.M. Torkar, W. Singer, I. Strelnikova, M. Rapp, and S. Robertson, Signatures of mesospheric particles in ionospheric data, *Ann. Geophys.*, 27, 823-829, 2009.
- Fujii, R., Y. Iwata, S. Oyama, S. Nozawa, and Y. Ogawa, Relations between proton auroras, intense electric field, and ionospheric electron density depletion, *J. Geophys. Res.*, 114, A09304, doi:10.1029/2009JA014319, 2009.
- Griffin, E.M., Aruliah, A.L., McWhirter, I., Yiu, H.-C.I., and Charalambous, A.: Upper thermospheric ion-neutral coupling from combined optical and radar experiments over Svalbard, *Ann. Geophys.*, 27, 4293-4303, 2009.
- Hartquist, T., O. Havnes and M. Kassa, Exploring polar mesospheric summer echoes, *Astronomy & Geophysics*, 50, 1, 1.08 - 1.14, 2009.
- Havnes, O., and M. Kassa, On the sizes and observable effects of dust particles in polar mesospheric winter echoes, *J. Geophys. Res.*, 114, D09209, doi:10.1029/2008JD011276, 2009.
- Havnes, O., M. Kassa, G.E. Morfill and C. La Hoz, On the sizes, charges and effects of dust particles in polar mesospheric winter echoes, *Proceedings of the 19th ESA Symposium on European rocket and Balloon Programmes and Related Research*, 7-11 June 2009, Bad Reichenhall, Germany, Esa publication, 2009.
- Havnes, O., C. La Hoz, M.T. Rietveld, M. Kassa, G. Baroni and A. Biebricher, Observation and analysis of polar mesospheric winter echoes modulated by artificial electron heating, *Proceedings of the 19th ESA Symposium on European rocket and Balloon Programmes and Related Research*, 7-11 June 2009, Bad Reichenhall, Germany, Esa publication, 2009.
- Kalogerakis, K.S., T.G. Slanger, E.A. Kendall, T.R. Pedersen, M.J. Kosch, B. Gustavsson, and M.T. Rietveld, Remote Oxygen Sensing by Ionospheric Excitation (ROSIE), *Ann. Geophys.*, 27, 2183-2189, 2009.
- Kozlovsky, A., T. Turunen, and S. Massetti, Field-aligned currents of postnoon auroral arcs, *J. Geophys. Res.*, 114, A03301, doi:10.1029/2008JA013666, 2009.
- Kurihara, J., Oyama, S. Nozawa, S., Tsuda, T.T., Fujii, R., Ogawa, Y., Miyaoka, H., Iwagami, N., Abe, T., Oyama, K.-I., Kosch, M., Aruliah, A., Griffin, E. , and K. Kauristie, K., Temperature enhancements and vertical winds in the lower thermosphere associated with auroral heating during the Dynamics and Energetics of the Lower thermosphere in Aurora (DELTA) campaign, *J. Geophys. Res.*, 114, A12306, doi:10.1029/2009JA014392, 2009.
- Lanchester, B.S., M. Ashrafi, N. Ivchenko, Simultaneous imaging of aurora on small scale in OI (777.4 nm) and N21P to estimate energy and flux of precipitation, *Annales Geophysicae* 27(7), 2881-2891, 2009.
- Leyser, T.B., and E. Nordblad, Self-focused radio frequency L wave pumping of localized upper hybrid oscillations in high-latitude ionospheric plasma, *Geophys. Res. Lett.*, 36, L24105, doi:10.1029/2009GL041438, 2009.
- Leyser, T.B., and A.Y. Wong, Powerful electromagnetic waves for active environmental research in geospace, *Rev. Geophys.*, 47, RG1001, doi:10.1029/2007RG000235, 2009.

- Li, Hailong, Study on the echo characteristics of Polar Mesosphere Summer Echoes, PhD thesis, Xidian University, China, 2009.
- Li Hailong, Wu Jian, Huang Jiying, Wang Maoyan, One analysis on the rocket detection of polar mesosphere summer echoes, *Chin. J. Space Sci.*, 29(4): 397-401, 2009a.
- Li Hailong, Wu Jian, Huang Jiying, WANG Maoyan, Study on the relation between the reflectivity and frequency in dusty plasma of polar summer mesopause, *Plasma Science and Technology*, 11(3): 279-282, 2009b.
- Li Hui Wu Jian Wu Jun Che Hai-Qing, Study on the Sharp Boundary of Layered Dust Structure in the Summer Polar Mesopause, *Chinese journal of polar research*, 21(4): 272-278, 2009.
- Lofas, H., N. Ivchenko, B. Gustavsson, T.B. Leyser, and M.T. Rietveld, F-region electron heating by X-mode radiowaves in underdense conditions, *Ann. Geophysicae*, 27, 2585-2592, 2009.
- Lunde, J., Particle Precipitation: Effects on Selected Ionospheric Phenomena, Ph.D thesis, University of Tromsø, Norway, 2009.
- Lunde, J., U. P. Løvhaug, and B. Gustavsson, Particle precipitation during NEIAL events: simultaneous ground based nighttime observations at Svalbard, *Ann. Geophys.*, 27, 2001-2010, 2009.
- Maeda, S., Y. Ogawa, K. Hosokawa, S. Nozawa, S. Oyama, T. Tsuda, and A. Brekke, Ion heating in high-speed flow channel within the duskside cell of the polar-cap ion convection under large IMF-By condition, *J. Geophys. Res.*, 114, A11307, doi:10.1029/2009JA014300, 2009.
- Ogawa, Y., S. C. Buchert, R. Fujii, S. Nozawa, and A. P. van Eyken, Characteristics of ion upflow and downflow observed with the European Incoherent Scatter Svalbard radar, *J. Geophys. Res.*, 114, A05305, doi:10.1029/2008JA013817, 2009.
- Ogawa, Y., I. Haggstrom, S. C. Buchert, K. Oksavik, S. Nozawa, M. Hirahara, A. P. van Eyken, T. Aso, and R. Fujii, On the source of the polar wind in the polar topside ionosphere: First results from the EISCAT Svalbard radar, *Geophys. Res. Lett.*, 36, L24103, doi:10.1029/2009GL041501, 2009.
- Osepian, A., S. Kirkwood, P. Dalin, and V. Tereschenko, D-region electron density and effective recombination coefficients during twilight - experimental data and modelling during solar proton events, *Ann. Geophys.*, 27, 3713-3724, 2009.
- Pitkänen, T., A.T. Aikio, A. Kozlovsky, and O. Amm, Reconnection electric field estimates and dynamics of high-latitude boundaries during a substorm, *Ann. Geophys.*, 27, 2157-2171, 2009.
- Rapp, M., I. Strelnikova, B. Strelnikov, R. Latteck, G. Baumgarten, Q. Li, L. Megner, J. Gumbel, M. Friedrich, U.-P. Hoppe, and S. Robertson, First in situ measurement of the vertical distribution of ice volume in a mesospheric ice cloud during the ECOMA/MASS rocket-campaign, *Ann. Geophys.*, 27, 755-766, 2009.
- Rentz, Stefanie, The Upper Atmospheric Fountain Effect in the Polar Cusp Region, PhD thesis, Fakultät für Elektrotechnik, Informationstechnik, Physik der Technischen Universität Carolo-Wilhelmina zu Braunschweig, Germany, 2009.
- Safargaleev, V.V., T.I. Sergienko, A.E. Kozlovsky, I. Sandahl, U. Brändström and D.N. Shibaeva, Electric field enhancement in an auroral arc according to the simultaneous radar (EISCAT) and optical (ALIS) observations, *Geomagnetism and Aeronomy*, 49, 3, 353-367, 2009.
- Sojka, J.J., R.L. McPherron, A.P. van Eyken, M.J. Nicolls, C.J. Heinselman, and J.D. Kelly, Observations of ionospheric heating during the passage of solar coronal hole fast streams, *Geophys. Res. Lett.*, 36, L19105, doi:10.1029/2009GL039064, 2009.
- Strelnikova, I., Mesospheric aerosol particles: Evidence from rocket and radar techniques, Ph.D. Thesis, Mathematisch-Naturwissenschaftlichen Fakultät der Universität Rostock, Germany, 2009.
- Strelnikova, I., M. Rapp, B. Strelnikov, G. Baumgarten, A. Brattli, K. Svenes, U.-P. Hoppe, M. Friedrich, J. Gumbel, B.P. Williams, Measurements of meteor smoke particles during the ECOMA-2006 campaign: 2. Results, *J. Atmos. Sol.-Terr. Phys.*, 71, 3-4, 486-496, 2009.
- Taguchi, S., S. Suzuki, K. Hosokawa, Y. Ogawa, A.S. Yukimatu, N. Sato, M.R. Collier, and T.E. Moore, Moving mesoscale plasma precipitation in the cusp, *J. Geophys. Res.*, 114, A06211, doi:10.1029/2009JA014128, 2009.
- Tsuda, T. T., S. Nozawa, S. Oyama, T. Motoba, Y. Ogawa, H. Shinagawa, N. Nishitani, K. Hosokawa, N. Sato, M. Lester, and R. Fujii, Acceleration mechanism of high-speed neutral wind observed in the polar lower thermosphere, *J. Geophys. Res.*, 114, A04322, doi:10.1029/2008JA013867, 2009.
- Vierinen, V., et al., Measuring space debris with phase coded aperiodic transmission sequences, *Proceedings of the 5th European Conference on Space Debris*, 2009.

Vierinen, V., and M. S. Lehtinen, 32-cm wavelength radar mapping of the moon, Proceedings of the 6th European Radar Conference, 2009.

Vierinen, J., J. Markkanen, and H. Krag, High power large aperture radar observations of the Iridium-Cosmos collision, Proceedings of the 10th Advanced Maui Optical and Space Surveillance Technologies Conference, 2009.

Virtanen, I., Multi-purpose Methods for Ionospheric Radar Measurements, Ph.D. Thesis, Department of Physics, University of Oulu, Finland, Report No. 59, Report Series in Physical Sciences, ISBN 978-951-42-9283-5, ISSN 1239-4327, Oulu University Press, Oulu 2009.

Virtanen, I.I., J. Vierinen, and M. S. Lehtinen, Phase-coded pulse aperiodic transmitter coding, *Ann. Geophys.*, 27, 2799-2811, 2009.

Wood, A.G., S. E. Pryse, and J. Moen, Modulation of nightside polar patches by substorm activity, *Ann. Geophys.*, 27, 3923-3932, 2009.

Xu, Bin, Study on the incoherent scatter spectra and its application in the ionospheric heating, PhD thesis, Xidian University, China, 2009.

Xu Bin, Wu Jian, Wu Zhensen and Xue Kun, Incoherent Scatter Spectra due to HF Heating in the Low Ionosphere Region, *Sci China Ser E-Tech Sci*, 52 (2): 1-5, 2009b.

Xu Bin, Wu Jun, Wu Jian, Wu Zhensen, Che Haiqin, Xu Zhengwen, Xue Kun, Yan Yubo, Observations of the heating experiments in the polar winter ionosphere, *Chinese Journal of Geophysics*, 52(4): 859-877, 2009c.

Xue, Kun, Theoretical and Experimental Study on the Incoherent Scatter Spectrum of High Latitude Auroral Ionosphere, PhD thesis, Xidian University, China, 2009.

Zalizovski, A.V., S.B. Kashcheyev, Y.M. Yampolski, V.G. Galushko, V. Belyey, B. Isham, M.T. Rietveld, C. La Hoz, A. Brekke, N.F. Blagoveshchenskaya, and V.A. Kornienko, Self-scattering of a powerful HF radio wave on stimulated ionospheric turbulence, *Radio Sci.*, 44, RS3010, doi:10.1029/2008RS004111., 2009.

EISCAT Operations 2009

The EISCAT radars operate in two basic modes, using approximately half the available observing time for each. In the Special Programme mode, users conduct individual experiments dedicated to specific experiments and objectives. The resulting data are reserved for the exclusive use of the experimenters for one year from the date of collection. Special programmes often make use of the well developed pulse schemes and observing modes of the Common Programme. EISCAT Common Programmes are conducted for the benefit of the entire user community and the resulting data are immediately available to all. The common Programme modes are developed and maintained by EISCAT staff, and the overall programme is monitored by the Scientific Advisory Committee. Common Programme operations are often conducted as part of the coordinated World Day programme organised by the International Union of Radio Scientists (URSI) Incoherent Scatter Working Group (ISWG).

Common Programme One, CP-1, uses a fixed transmitting antenna, pointing along the geomagnetic field direction. The three-dimensional velocity and anisotropy in other parameters are measured by means of the receiving stations at Kiruna and Sodankylä (see map, inside front cover). CP-1 is capable of providing results with very good time resolution and is suitable for the study of substorm phenomena, particularly auroral processes where conditions might change rapidly. The basic time resolution is 5 s. Continuous electric field measurements are derived from the tri-static F-region data. On longer time scales, CP-1 measurements support studies of diurnal changes, such as atmospheric tides, as well as seasonal and solar-cycle variations. The observation scheme uses alternating codes for spectral measurements.

Common Programme Two, CP-2, is designed to make measurements from a small, rapid transmitter antenna scan. One aim is to identify wave-like phenomena with length and time scales comparable with, or larger than, the scan (a few tens of kilometers and about ten minutes). The present version consists of a four-position scan which is

completed in six minutes. The first three positions form a triangle with vertical, south, and south-east positions, while the fourth is aligned with the geomagnetic field. The remote site antennas provide three-dimensional velocity measurements in the F-region. The pulse scheme is identical with that of CP-1.

Common Programme Three, CP-3, covers a 10° latitudinal range in the F-region with a 17-position scan up to 74°N in a 30 minute cycle. The observations are made in a plane defined by the magnetic meridian through Tromsø, with the remote site antennas making continuous measurements at 275 km altitude. The coding scheme uses alternating codes. The principle aim of CP-3 is the mapping of ionospheric and electrodynamic parameters over a broad latitude range.

Common Programmes One, Two, and Three are run on the UHF radar. Three further programmes are designed for use with the VHF system. The UHF and VHF radars are often operated simultaneously during the CP experiments. Such observations offer comprehensive data sets for atmospheric, ionospheric, and magnetospheric studies.

Common Programme Four, CP-4, covers geographic latitudes up to almost 80°N (77°N invariant latitude) using a low elevation, split-beam configuration. CP-4 is particularly suitable for studies of high latitude plasma convection and polar cap phenomena.

Common Programme Six, CP-6, is designed for low altitude studies, providing spectral measurements at mesospheric heights. Velocity and electron density are derived from the measurements and the spectra contain information on the aeronomy of the mesosphere. Vertical antenna pointing is normally used.

Common Programme Seven, CP-7, probes high altitudes and is particularly aimed at polar wind studies. The present version uses both of the VHF klystrons and is designed to cover altitudes up to 2500 km vertically above Ramfjordmoen.

Equivalent Common Programme modes are available for the EISCAT Svalbard Radar. CP-1 is directed along the geomagnetic field (81.6° in-

clination). CP-2 uses a four position scan. CP-3 is a 15 position elevation scan with southerly beam swinging positions. CP4 combines observations in the F-region viewing area with field-aligned and vertical measurements. Alternating code pulse schemes have been used extensively for each mode to cover ranges of approximately 80 to 1200 km with integral clutter removal below 150 km.

The tables on the next pages summarise the accounted hours on the various facilities for each month and for each Common Programme mode (CP) or Associate (SP).

KST COMMON PROGRAMMES

2009	Jan	Feb	Mar	Apr	May	Jun	Jul	Aug	Sept	Oct	Nov	Dec	Total	%	Target%
CP1		7.5	5	3	102.5								118	13	16
CP2	87.5								352.5				440	47	16
CP3			80.5									135	215.5	23	12
CP4													0	0	10
CP6		32.5				87.5	11						131	14	20
CP7													0	0	18
UP1		24.5											24.5	3	
UP2													0	0	
UP3													0	0	
Total	87.5	64.5	85.5	3	102.5	87.5	11	0	352.5	0	0	135	929	100	
%	9	7	9	0	11	9	1	0	38	0	0	15	100		

KST SPECIAL PROGRAMMES

2009	Jan	Feb	Mar	Apr	May	Jun	Jul	Aug	Sept	Oct	Nov	Dec	Total	Incl AA	Target
CN								132					132	135	51
FI	15				31						36	87	169	174	86
GE	13.5		14.5			16	15					16	75	78	50
NI	32.5		6							11	46		95.5	101	102
NO	33		12.5				72.5	6			10	100	234	245	196
SW	21									35.5	154.5		211	219	141
UK	6.5		47.5			21	24.5	2					101.5	109	132
AA			27						16				43		
Total	121.5	0	107.5	0	31	37	112	140	16	46.5	246.5	203	1061	1061	758
%	11	0	10	0	3	3	11	13	2	4	23	19	100		

	EI	CN	FI	GE	NI	NO	SW	UK	%
Target		6.7	11.4	6.56	13.41	25.91	18.6	17.43	

KST OTHER PROGRAMMES

2009	Jan	Feb	Mar	Apr	May	Jun	Jul	Aug	Sept	Oct	Nov	Dec	Total	Target
3P	8						18.5	1					27.5	15
EI											0.5	8	8.5	31
TNA						35			85		67.5	101	288.5	120
TB	11.5		63.5							25	54.5	48.5	203	203
Total	19.5	0	63.5	0	0	35	18.5	1	85	25	122.5	157.5	527.5	369

KST CUMULATIVE TOTALS

2009	Jan	Feb	Mar	Apr	May	Jun	Jul	Aug	Sept	Oct	Nov	Dec	Total	Target
CP	87.5	64.5	85.5	3	102.5	87.5	11	0	352.5	0	0	135	929	980
SP	121.5	0	107.5	0	31	37	112	140	16	46.5	246.5	203	1061	758
OP	19.5	0	63.5	0	0	35	18.5	1	85	25	122.5	157.5	527.5	369
Total	228.5	64.5	256.5	3	133.5	159.5	141.5	141	453.5	71.5	369	495.5	2517.5	2107

USAGE BREAKDOWN

2009	Jan	Feb	Mar	Apr	May	Jun	Jul	Aug	Sept	Oct	Nov	Dec	Total	Target
UHF	179	29.5	131.5	3	75.5	108	42	60	278.5	44.5	215.5	257	1424	856
VHF	14	32.5	49.5			8	70	28	16		40	128	386	363
Heating			46				30	50.5	19	12.5	26.5	13.5	198	285
Passive UHF	142	11	119		133	177.5		9.5	560	58.5	346.5	374.5	1931.5	2414
ESR	126.5	120	98.5	11.5	82	108	0	33.5	267.5	21	0	287.5	1156	1342
Passive ESR						58							58	

ESR COMMON PROGRAMMES

2009	Jan	Feb	Mar	Apr	May	Jun	Jul	Aug	Sept	Oct	Nov	Dec	Total	%	Target%
CP1	3	82.5		0.5	54				1.5				141.5	21	54
CP2	30.5		49						254.5				334	50	16
CP3												103	103	15	12
CP4													0	0	10
CP6		2.5	1.5			83.5							87.5	13	
CP7				1.5									1.5	0	
UP1													0	0	
UP2													0	0	
UP3													0	0	
Total	33.5	85	50.5	2	54	83.5	0	0	256	0	0	103	667.5	100	
%	5	13	8	0	8	13	0	0	38	0	0	15	100		

ESR SPECIAL PROGRAMMES

2009	Jan	Feb	Mar	Apr	May	Jun	Jul	Aug	Sept	Oct	Nov	Dec	Total	Incl AA	Target
CN													0	4	34
FI	4											22.5	26.5	33	58
GE						15							15	19	33
NI								33.5		21		7	61.5	69	68
NO	8		10	9.5	28	9.5						29.5	94.5	110	132
SW	14.5											30	44.5	56	95
UK	57.5	13	12			14.5							97	107	89
AA		22	26						11.5				59.5		
Total	84	35	48	9.5	28	39	0	33.5	11.5	21	0	89	398.5	399	509
%	21	9	12	2	7	10	0	8	3	5	0	22	100		

ESR OTHER PROGRAMMES

2009	Jan	Feb	Mar	Apr	May	Jun	Jul	Aug	Sept	Oct	Nov	Dec	Total	Target
3P	9												9	12
EI													0	25
TNA													0	
TB												95.5	95.5	96
Total	9	0	0	0	0	0	0	0	0	0	0	95.5	104.5	133

ESR CUMULATIVE TOTALS

2009	Jan	Feb	Mar	Apr	May	Jun	Jul	Aug	Sept	Oct	Nov	Dec	Total	Target
CP	33.5	85	50.5	2	54	83.5	0	0	256	0	0	103	667.5	700
SP	84	35	48	9.5	28	39	0	33.5	11.5	21	0	89	398.5	509
OP	9	0	0	0	0	0	0	0	0	0	0	95.5	104.5	133
Total	126.5	120	98.5	11.5	82	122.5	0	33.5	267.5	21	0	287.5	1170.5	1342

Beynon medals



The EISCAT Council awards distinguished persons the Sir Granville Beynon medal.

Recipients

1st Prof. Tor Hagfors 2002 Awarded to Professor Tor Hagfors on 4th February 2002 for his outstanding services to the EISCAT Scientific Association and to Ionospheric Physics

2nd Prof. Tauno Turunen 2003 In recognition of important contributions to the techniques of Incoherent Scatter Radar and outstanding services to the EISCAT Scientific Association

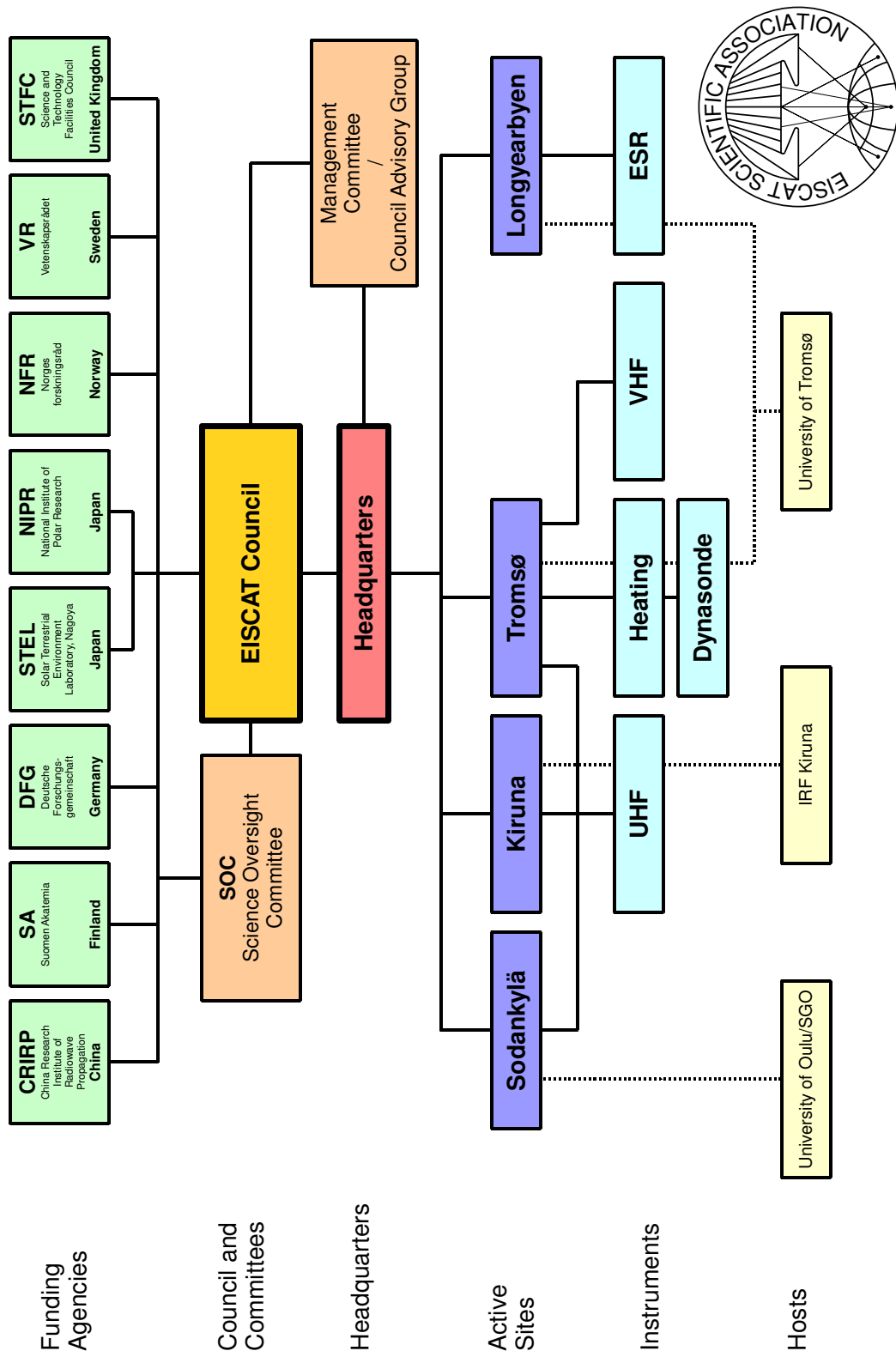
3rd Prof. Jürgen Röttger 2004 In recognition of outstanding services to the EISCAT Scientific Association including the establishment of the EISCAT Svalbard Radar at Longyearbyen

4th Prof. Henry Rishbeth 2006 Awarded by the Council of the EISCAT Scientific Association to Professor Henry Rishbeth. In recognition of outstanding contributions to the scientific exploitation of incoherent scatter in Europe including the UK PUSCAT and MISCAT radars and the radars of the EISCAT Scientific Association

5th Prof. Nobuo Matuura 2007 Awarded by the Council of the EISCAT Scientific Association to Professor Nobuo Matuura. In recognition of his contributions to the successful establishment of the EISCAT Svalbard Radar at Longyearbyen and to the expansion of the EISCAT Scientific Association to include non-European members

6th Prof. Markku Lehtinen 2008 Awarded by the Council of the EISCAT Scientific Association to Professor Markku Lehtinen. In recognition of his seminal contributions to the development of advanced modulation techniques for incoherent scatter radars and to the mathematical foundations and implementation of effective incoherent scatter radar data analysis systems

7th Dr. Gudmund Wannberg 2009 Awarded by the Council of the EISCAT Scientific Association to Doctor Gudmund Wannberg. In recognition of his persistent work for the technical development of EISCAT radars and his invaluable contribution to the EU Design Study project for the EISCAT_3D radars.



EISCAT organisational diagram, December 2009.

EISCAT Scientific Association

December 2009

Council

The Council consists of a Delegation of each Associate with a maximum of three persons from each Associate.

Finland

Dr. K. Kauristie *Chairperson*
Prof. T. Nygrén
Dr. K. Sulonen Delegate

Germany

Dr. H. Boos Delegate
Prof. J. Röttger

Japan

Prof. R. Fujii Delegate
Dr. H. Miyaoka Delegate

Norway

Prof. A. Brekke
Dr. B. Jacobsen Delegate
Dr. L. Lønnum

Sweden

Dr. T. Andersson *Vice-Chairperson, Delegate*
Prof. D. Murtagh

P. R. of China

Prof. Q. Dong Delegate
Prof. J. Wu

United Kingdom

Dr. I. McCrea
Ms. R. Young Delegate

Director

Dr. E. Turunen

Council Advisory Group

Towards the end of the year the previous Management Committee was reformed into the Council Advisory Group. Its members were not yet finalised in December 2009, the list here is of the acting members.

Mr. H. Andersson	Head of Administration
Dr. T. Andersson	Council Vice-Chairperson
Prof. A. Brekke	Council Member
Dr. K. Kauristie	Council Chairperson
Dr. E. Turunen	Director

Executives

Senior Management

Mr. H. Andersson	Head of Adm., Deputy Dir.
Dr. E. Turunen	Director

Site Leaders

Station Managers

Mr. H. Boholm	EISCAT Svalbard Radar
Mr. R. Jacobsen	Tromsø Radar
Mr. M. J. Postila	Sodankylä Site
Dr. M. T. Rietveld	Tromsø Heating
Mr. L.-G. Vanhainen	Kiruna Site

Scientific Oversight Committee

Under the guidance of the Council, the EISCAT scientific community organises a Scientific Oversight Committee.

Dr. A. Aikio	Finland
Dr. N. Blagoveshchenskaya	External member
Dr. S. Buchert	Sweden
Dr. J. Chau	External member
Dr. M. Kosch	United Kingdom
Prof. C. La Hoz	Norway
Prof. R. Liu	<i>Chairperson, P. R. of China</i>
Prof. S. Nozawa	Japan
Prof. J. Röttger	Germany



EISCAT staff at the Annual Review Meeting, 11–13 February 2009, at Pallastunturi, Finland.

Appendix:

**EISCAT Scientific Association
Annual Report, 2009**

EISCAT Scientific Association Annual Report 2009

EISCAT Scientific Association
Registered as a Swedish non-profit organisation
Organisation number: 897300-2549

Annual report for the financial year 2009-01-01 – 2009-12-31

The EISCAT Council and the Director for the Association herewith submits the annual report for 2009.

Content	Page
Administration report	1
Profit and loss accounts	5
Balance sheet	6
Statement of cash flows	7
Notes	8

ADMINISTRATION REPORT

Ownership, organisation and objective

The EISCAT Scientific Association was established in 1975 through an agreement between six European organisations. Japan joined in 1996 and the Peoples Republic of China in 2007.

The EISCAT Associates at 2009-12-31 are: China Research Institute of Radiowave Propagation (Peoples Republic of China), Deutsche Forschungsgemeinschaft (Germany), National Institute of Polar Research (Japan), Norges forskningsråd (Norway), Science and Technology Facilities Council (United Kingdom of Great Britain and Northern Ireland), Solar-Terrestrial Environment Laboratory, Nagoya University (Japan), Suomen Akatemia (Finland), and Vetenskapsrådet (Sweden).

A new EISCAT Agreement came into force 2007-01-01, with all Associates making long term funding commitments to the Association. The Association has its formal seat in Kiruna, Sweden, and is registered as a non-profit organisation.

The aim of the Association is to make significant progress in the understanding of physical processes in the high latitude atmosphere by means of experimental programmes generally conducted using the incoherent scatter radar technique, which may be carried out as part of wider international projects. For this purpose, the Association has developed, constructed, and now operates, a number of radar facilities at high latitudes. At present, these comprise a system of stations at Tromsø (Norway), Kiruna (Sweden), Sodankylä (Finland), and Longyearbyen (Svalbard).

The Association is fully funded by the Associates but additional operations may also be funded by short term additional contributions from both Associate and non-Associate bodies. Depending on the available funding, scientific priorities and operational targets are adjusted on an annual basis.

The EISCAT Council is charged with the overall administration and supervision of the Association's activities. The Council appoints a Director, who is responsible for the daily management and operation of the facilities of the Association.

Operation and scientific development

The EISCAT Radars delivered a full programme of operations for the user community and operated reliably throughout the year with only minor interruptions due to equipment or operational problems.

The various EISCAT radars operated for a total of 3 688 accounted hours (5 209 hours in 2008).

Common Programmes amounted to 43% (34%) of the operations. Special Programmes amounted to 40% (34%) and other operations, such as the TNA project runs, amounted to 17% (32%) of the total run hours.

Both contracts under the European Union's Sixth Framework Programme initiative, the EISCAT_3D design study and the Transnational Access project ended during the year.

Both projects were completed in a proper manner. The EISCAT_3D project planning continues and a bid for the European Union's Seventh Framework Programme, ESFRI projects preparatory phase, was submitted in December.

The Transnational Access project funded six user campaigns and 195 hours (92 hours) of operation during the final period of the four year project.

Scientists from France, Ukraine and Russia paid for the use of the facilities. Totally 298.5 hours (211.5 hours) were run on behalf of these affiliated countries.

The annual staff review meeting was held in Pallastunturi, Finland, mid February. EISCAT scientists attended several international conferences during the year. The EISCAT_3D continued work, including setting up the new consortium that submitted the preparatory project bid, and promotion trips also meant frequent travel. The number of travel days increased by about 50% in 2009.

Future operation and scientific development

During the coming year, EISCAT will continue to support the wide range of existing and new programmes proposed by the various Associates' scientific communities, including the hosting of user-supplied equipment.

It is though expected that UHF tristatic runs will no longer be possible beyond July 2010 since the required disturbance free frequency slots in Finland and Sweden will be taken in use by mobile phone operators. In Sweden, the operators will have access to the frequency spectrum 1 March 2010 and in Finland 1 January 2010, though it has been stated that the Finnish operator will only start using it near the Finnish site 1 July 2010 and the Swedish one perhaps not at all in 2010.

Ways of continuing tristatic capabilities are considered. The primary option is the planned EISCAT_3D system which will give full three-dimensional capabilities. Since the EISCAT_3D project is still years from build, intermediate steps are evaluated which could fill some scientific requirements, like meteor studies, while waiting for the new system.

The three other radar systems, UHF in monostatic mode, VHF and the Svalbard Radar continues undisturbed. The Heating facility has recently been modernised and its extended capabilities allows for new experimental modes.

The work of the Council and its committees

The Council had two ordinary and one extraordinary meeting under the leadership of the Chairperson, Dr. Kirsti Kauristie: in June, Berlin, Germany and in October, Lillehammer, Norway. An extraordinary telephone conference meeting was held as in December.

The management committee had two meetings: in May, Longyearbyen, Svalbard and in September, Sodankylä, Finland.

The Scientific Oversight Committee had two meetings during the year: March, Kühlungsborn, Germany and in September, Arecibo, Puerto Rico.

Council considered mainly regular business matters. The transfer of Associateship from UK's Science and Technology Facilities Council (STFC) to the Natural Environment Research Council (NERC) resulted in the extraordinary meeting. The addressed issue, the length of the UK commitment at the time of transfer, is now resolved.

Council decided also to change the remit of the management committee such that it becomes an advisory group for Council. The new Council Advisory Group is headed by the Council Chairperson and will provide guidance and advice to Council.

Budget development during the year

The 2009 operations ended very close to the operating target set for the year. Both EU supported projects ended during the year. Both were four year projects and both ended as envisaged though bit below the initial budget total.

French and Ukrainian scientists took advantage, against payment, of the systems. It is anticipated that both countries, and Russia, will continue to make use of the systems also in the coming years.

Most of the regular Associates, Finland, Japan, Norway, P. R. of China, Sweden and United Kingdom agreed to add an inflationary compensation to their annual contributions in 2009. In addition, since the contributions are in local currencies, the income side benefited from the relatively weak SEK-currency. Due to low global interest levels, the budgeted bank interest on own funds did not meet the target.

The continued EISCAT_3D work resulted in a bid for a preparatory phase, under the EU Framework Programme 7 initiative. The application was submitted in December 2009 and the first evaluation results look promising.

The long-term budget plan

The long-term budget plan is becoming challenging due to the current known funding shortage from 2012 onwards. For 2010 and 2011, we do not anticipate any issues other than the reported trisatic problem and the overall operating target for these years can be maintained.

The result for 2009 and the deficit handling

The year was balanced by transferring the surplus, relative to the budget, of 3 415 kSEK, to the investment fund.

PROFIT AND LOSS ACCOUNTS

in thousands of Swedish Crowns

	Note 1	2009	2008
Associate contributions	Note 2	26 586	23 611
Other operating income		6 180	8 592
		<u>32 766</u>	<u>32 203</u>
Operation costs		-5 257	-6 361
Administration costs		-4 517	-4 253
Personnel costs	Note 3	-17 706	-23 956
Depreciation of fixed assets		-2 198	-5 026
		<u>-29 677</u>	<u>-39 596</u>
<i>Operating profit/loss</i>		<i>3 089</i>	<i>-7 393</i>
Interest income		85	866
Other financial income and cost		-622	351
Own reserves and funds	Note 4	-1 335	-145
		<u>-1 871</u>	<u>1 072</u>
<i>Profit/loss after financial items</i>		<i>1 217</i>	<i>-6 321</i>
Appropriations	Note 5	-3 415	1 295
Transfer from funds invested	Note 6	2 198	5 026
		<u>-1 217</u>	<u>6 321</u>
<i>Net profit/loss for the year</i>		<i>0</i>	<i>0</i>

BALANCE SHEET

in thousands of Swedish Crowns

		2009	2008
ASSETS			
<u>Fixed assets</u>			
<i>Tangible fixed assets</i>	Note 7		
Buildings		3 843	3 995
Radar systems		821	2 041
Equipment and tools		2 099	1 643
		<u>6 764</u>	<u>7 679</u>
<u>Current assets</u>			
Receivables		3 871	1 723
Prepayments and accrued income	Note 8	640	610
Cash at bank and in hand	Note 9	19 222	20 370
		<u>23 733</u>	<u>22 703</u>
<i>Total assets</i>		30 496	30 383
CAPITAL AND LIABILITIES			
<u>Capital</u>			
Funds invested	Note 10	6 764	7 108
Funds held on reserve	Note 11	18 763	16 053
		<u>25 526</u>	<u>23 161</u>
<u>Long term liabilities</u>			
Long term liabilities	Note 12	0	509
<u>Current liabilities</u>			
Liabilities, trade	Note 13	4 469	4 768
Provisions	Note 14	155	37
Other liabilities		345	1 908
		<u>4 970</u>	<u>6 713</u>
<i>Total capital and liabilities</i>		30 496	30 383
<i>Pledged assets</i>		0	509
<i>Contingent liabilities</i>		none	none

STATEMENT OF CASH FLOWS

in thousands of Swedish Crowns

	2009	2008
<u>Operating activities</u>		
Operating result before financial items	3 089	-7 393
Transfer from funds invested	2 198	5 026
Interest received	85	866
Currency exchange rate changes	-658	314
Extra ordinary income and cost	36	37
Increase/decrease of receivables	-2 148	878
Increase/decrease of prepayments and accrued income	-30	5
Increase/decrease of creditors and liabilities	-2 252	-11 364
<i>Cash flow from operations</i>	<i>321</i>	<i>-11 631</i>
<u>Investment activities</u>		
Investments in tangible assets	-1 469	-908
<i>Cash flow from investment activities</i>	<i>-1 469</i>	<i>-908</i>
<i>Cash flow for the year</i>	<i>-1 148</i>	<i>-12 539</i>
<i>Liquid assets at the beginning of the year</i>	<i>20 370</i>	<i>32 909</i>
<i>Liquid assets at the end of the year</i>	<i>19 222</i>	<i>20 370</i>

EISCAT Scientific Association Annual Report 2009

NOTES

Note 1 Accounting principles

The accounting and valuation principles applied are consistent with the provisions of the Swedish Annual Accounts Act and generally accepted accounting principles (bokföringsnämnden allmänna råd och vägledningar).

All amounts are in thousands of Swedish kronor (SEK) unless otherwise stated.

Receivables

Receivables are stated at the amounts estimated to be received, based on individual assessment.

Receivables and payables in foreign currencies

Receivables and payables in foreign currencies are valued at the closing day rate. Where hedging measures have been used, such as forwarding contracts, the agreed exchange rate is applied. Gains and losses relating to operations are accounted for under other financial income and cost.

Bank accounts in foreign currencies

Bank balances in foreign currencies are valued at the closing day rate.

Fixed assets

Tangible fixed assets are stated at their original acquisition values after deduction of depreciation according to plan. Assets are depreciated systematically over their estimated useful lives. The following periods of depreciation are applied: Buildings 5 - 50 years, Radar systems 3 - 20 years and Equipment and tools 1 - 5 years.

Note 2 Associate contributions

The Associates contributed to the operation during the year in accordance with the agreement. The commitments are in local currencies. The received contributions have been accounted in SEK.

	<u>2009</u>
CRIRP (P. R. of China)	3 129
DFG (Germany)	1 964
NIPR (Japan)	1 820
RCN (Norway)	6 010
SA (Finland)	3 996
STFC (United Kingdom)	4 039
VR (Sweden)	5 628
	<u>26 586</u>

Accumulated contributions status as of 2009-12-31

	<u>1976 - 2009</u>
Previous Associates	190 074
CRIRP (P. R. of China)	10 609
DFG (Germany)	188 749
NIPR (Japan)	66 904
RCN (Norway)	134 376
SA (Finland)	58 817
STFC (United Kingdom)	214 391
VR (Sweden)	108 029
	<u>971 948</u>

Note 3 Personnel costs and average number of employees

The Association employs directly the Headquarters staff, currently about six positions, including the Director. The Headquarters is located in Kiruna, Sweden. The personnel working at the Kiruna (Sweden), Sodankylä (Finland), Svalbard and Tromsö (Norway) sites are not employed by the Association. Instead, the personnel are provided via site contracts by the Swedish Institute of Space Physics (Kiruna site staff), Oulu University (Sodankylä staff) and Tromsö University (Tromsö and Svalbard staff). The Association refunds all expenses related to the provided staff, as well as an additional overhead.

Personnel costs in total

	<u>2009</u>	<u>2008</u>
Salaries and emoluments paid to the Directors	1 240	6 583
Other personnel, employed and provided via site contracts	11 031	11 472
Social security contributions amounted to of which for pension costs	3 944	4 717
	1 992	3 170

The new Director, Dr. Esa Turunen, started his employment 2009-01-01. His employment contract with Council is for three years.

Of the pension costs, 320 kSEK (previous directors 1 660 kSEK) relates to the Director. He and all other directly employed staff are included in ITP like occupational pension plans. For the personnel provided via site contracts, the pension plans are handled by their respective employer.

The members of the board (EISCAT Council) and members of committees, who represents Associates, do not receive remunerations from the Association. Travel expenses in connection with Council and committee meetings are normally covered by the Associates. For the Council Advisory Group (earlier named Management Committee), the Association cover meeting and travel costs.

Salaries and emoluments and average number of staff per country

Finland		
Salaries and emoluments	1 528	1 767
Average number of staff - men and women	3 + 0	4 + 0
Norway (including Svalbard)		
Salaries and emoluments	5 370	12 033
Average number of staff - men and women	9 + 0	10 + 1
Sweden		
Salaries and emoluments	5 372	4 255
Average number of staff - men and women	8 + 1	6 + 1

Members of the board and Directors at year-end - men and women

The board consist of delegations from every Associate country each having a Delegate (formal member) and up to two Representatives.

Board members (EISCAT Council)	12 + 4	12 + 4
Directors	1 + 0	2 + 0

Note 4 Own reserves and funds

Transactions involving own reserves and funds.

Capital Operating reserve		
Budgeted transfer to the reserve	-1 614	-396
Transfer from the reserve	1 469	908
Investments made	-2 040	-942

External projects reserve

Design study project complete, contingency released

	1 504	-675
--	-------	------

Restructuring reserve

Budgeted restructuring costs

	1 500	1 355
--	-------	-------

Spare parts reserve

Budgeted transfer to the reserve

	-28	-27
Transfer from the reserve	9	9

EISCAT Scientific Association Annual Report 2009

	2009	2008		2009	2008
Investment fund			Note 8 Prepayments and accrued income		
Budgeted transfer to the fund	-2 000	0	The main buildings and systems insurance for 2009 was paid in December.		
Surplus fund			Prepaid rents	91	92
Budgeted transfer from the fund	4 062	3 685	Prepaid insurances	460	492
Budgeted transfer to the fund	-4 196	-4 062	Other items	89	26
<i>Sum own reserves and funds</i>	-1 335	-145		<u>640</u>	<u>610</u>
Note 5 Appropriations			Note 9 Bank balances status		
The outcome for this year became a surplus relative to the budget amounting to 3 415 kSEK. The amount has been transferred to the Investment fund. The 2008 outcome was a loss (-1 295 kSEK) which was covered by funds from the Restructuring reserve.			Nordea	19 220	20 369
Note 6 Transfer from funds invested			Cash in hand	2	1
The depreciation cost is covered by funds from Capital - funds invested				<u>19 222</u>	<u>20 370</u>
Note 7 Tangible fixed assets			Note 10 Funds invested status		
Changes in tangible fixed assets during 2009.			Buildings	3 843	3 424
Buildings			Radar Systems	821	2 041
Opening acquisition value	42 237	42 237	Equipment and Tools	2 099	1 643
Acquisitions during the year	137	0		<u>6 764</u>	<u>7 108</u>
Disposals during the year	0	0	Note 11 Funds held on reserve		
Closing acquisition value	42 374	42 237	Investments were made a bit below the budgeted expectation. Less spare parts than budgeted were acquired. Since the EISCAT_3D design study ended close to the planned target, the External project reserve did not need to be used and the funds were released. The positive outcome of this year (3 415 kSEK) has been put into the Investment fund. The other transfers were as budgeted.		
Opening accumulated depreciation	-38 242	-37 956	Capital operating reserve	1 369	1 223
Depreciations during the year	-289	-286	Equipment repair fund	754	754
Disposals during the year	0	0	External projects reserve	0	1 504
Closing accumulated depreciation	-38 531	-38 242	Investment fund	7 971	2 556
Closing residual value	3 843	3 995	Restructuring reserve	4 101	5 601
Radar systems			Spare parts reserve	371	353
Opening acquisition value	244 381	244 381	Surplus fund	4 196	4 062
Acquisitions during the year	103	0		<u>18 763</u>	<u>16 053</u>
Disposals during the year	0	0	Note 12 Long term liabilities		
Closing acquisition value	244 484	244 381	Husbanken Norway loan concerning the owned flat on Svalbard was paid-off during the year. In 2008 the loan was amortized (34 kSEK).		
Opening accumulated depreciation	-242 340	-238 389	Note 13 Liabilities, trade		
Depreciations during the year	-1 323	-3 951	Both EU-contracts, the EISCAT_3D Design Study and the EISCAT_USERS_1 Transnational access project ended during the year. In 2008, non released funds were accounted as liabilities.		
Disposals during the year	0	0	Liabilities EU, EISCAT_3D pre-financing	0	0
Closing accumulated depreciation	-243 662	-242 340	Liabilities EU, USERS_1 pre-financing	0	913
Closing residual value	821	2 041	Other liabilities, trade	4 469	3 855
Equipment and tools				<u>4 469</u>	<u>4 768</u>
Opening acquisition value	31 925	31 078	Note 14 Provisions		
Acquisitions during the year	1 229	908	The electricity provider on Svalbard did an erroronus cost debit Q1 2009. It is assumed that it will be corrected when settling the year.		
Disposals during the year	-98	-61	Council cost	0	37
Closing acquisition value	33 057	31 925	Electricity cost	155	0
Opening accumulated depreciation	-30 283	-29 442		<u>155</u>	<u>37</u>
Depreciations during the year	-586	-789			
Disposals during the year	-89	-52			
Closing accumulated depreciation	-30 958	-30 283			
Closing residual value	2 099	1 643			
<i>Sum tangible fixed assets</i>	6 764	7 679			

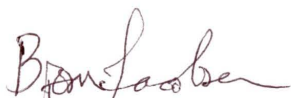
Tokyo 2010-06-03



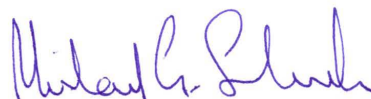
Dr. Tomas Andersson



Prof. Ryoichi Fujii



Dr. Bjørn Jacobsen

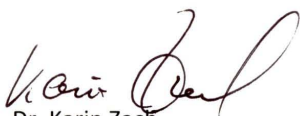


Dr. Michael Schultz



Dr. Kati Sulonen

Prof. Jian Wu



Dr. Karin Zach



Dr. Esa Turunen
Director

Our audit report was issued on 2010-06-14



Mrs. Annika Wedin
Authorised Public Accountant

Öhrlings

PRICEWATERHOUSECOOPERS 

Audit report

To the council of EISCAT Scientific Association

Corporate identity number 897300-2549

I have audited the annual accounts, the accounting records and the administration of the council and the director of EISCAT Scientific Association for the year 2009. These accounts and the administration of the association and the application of the Annual Accounts Act when preparing the annual accounts are the responsibility of the council and the director. My responsibility is to express an opinion on the annual accounts and the administration based on my audit.

I conducted my audit in accordance with generally accepted auditing standards in Sweden. Those standards require that I plan and perform the audit to obtain reasonable assurance that the annual accounts are free of material misstatement. An audit includes examining, on a test basis, evidence supporting the amounts and disclosures in the accounts. An audit also includes assessing the accounting principles used and their application by the council and the director and significant estimates made by the council and the director when preparing the annual accounts as well as evaluating the overall presentation of information in the annual accounts. As a basis for my opinion concerning discharge from liability, I examined significant decisions, actions taken and circumstances of the association in order to be able to determine the liability, if any, to the council or the director. I also examined whether any council member or the director has, in any other way, acted in contravention of the Annual Accounts Act or the statutes. I believe that my audit provides a reasonable basis for my opinion set out below.

The annual accounts have been prepared in accordance with the Annual Accounts Act and give a true and fair view of the association's financial position and results of operations in accordance with generally accepted accounting principles in Sweden.

The statutory administration report is consistent with the other parts of the annual accounts.

The council and the director have not acted in contravention of the statutes.

Gävle, 14 June 2010



Annika Wedin
Authorized Public Accountant

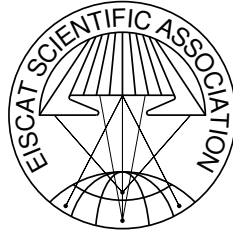
Report 2009 of the EISCAT Scientific Association

©EISCAT Scientific Association

EISCAT Headquarters

Box 812, SE-981 28 Kiruna, Sweden

Scientific contributions: EISCAT Associates and staff



The EISCAT Associates

December 2009

CRIRP

China Research Institute of Radiowave Propagation
China
www.crip.ac.cn

SA

Suomen Akatemia
Finland
www.aka.fi

DFG

Deutsche Forschungsgemeinschaft
Germany
www.dfg.de

STEL

Solar Terrestrial Environment Laboratory, Nagoya
Japan
www.stelab.nagoya-u.ac.jp

NIPR

National Institute of Polar Research
Japan
www.nipr.ac.jp

NFR

Norges forskningsråd
Norway
www.forskningsradet.no

VR

Vetenskapsrådet
Sweden
www.vr.se

STFC

Science and Technology Facilities Council
United Kingdom
www.scitech.ac.uk

EISCAT Scientific Association

Headquarters

EISCAT Scientific Association
Box 812
SE-981 28 Kiruna, Sweden
Phone: +46 980 79150
Fax: +46 980 79159
www.eiscat.se

Sites

Kiruna

EISCAT Kiruna Site
Box 812
SE-981 28 Kiruna, Sweden
Phone: +46 980 79136
Fax: +46 980 29276

Sodankylä

EISCAT Sodankylä Site
Tähteläntie 54B
FIN-99600 Sodankylä, Finland
Phone: +358 16 619880
Fax: +358 16 610375

Tromsø

EISCAT Tromsø Site
Ramfjordmoen
N-9027 Ramfjordbotn, Norway
Phone: +47 776 20730
Fax: +47 776 20740

Longyearbyen

EISCAT Svalbard Radar
Postboks 432
N-9171 Longyearbyen, Svalbard
Phone: +47 790 21236
Fax: +47 790 21751